4.6 DC resistivity and IP field systems, data processing and interpretation

- Electrode arrays
- Response of a layered earth
- The impact of small scale near surface inhomogeneities
- Detection and resolution of thin layers
- The anisotropic half-space
- Solutions for arbitrary conductivity distribution
- The general two-dimensional model
- Practical considerations

Return to top

Electrode arrays

a) Pole-Pole
b) Pole-Dipole
c) Wenner
d) Schlumberger
e) Dipole-Dipole
f) Data plotting for the pole-pole, pole-dipole and dipole-dipole arrays

All the arrays of electrodes used to obtain the apparent resistivity are variants of the four-electrode scheme that was introduced in section 4.3. All the arrays are basically superpositions of the fundamental equation for the potential from a current source with appropriate sign for the current. The formulas for apparent resistivity are a product of the impedance V/I (Ohms) and a geometric

factor with the units of length (meters). To investigate the resistivity distribution with depth, called a sounding, the arrays are expanded about a center point and the apparent resistivities are plotted vs. spacing usually on a log-log plot. In the more general case the apparent resistivities are plotted as a function of array spacing and lateral position using plotting conventions that have become accepted for each type of array.

a) <u>Pole-Pole</u>

The simplest array is one in which one of the current electrodes and one of the potential electrodes are placed so far away that they can be considered at infinity. This configuration with its formula for apparent resistivity is shown below.

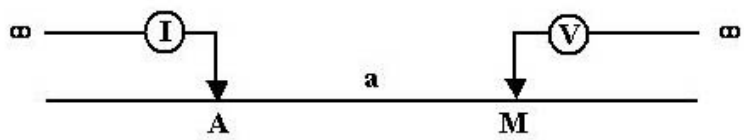

$$\rho_A = \frac{V}{I} 2\pi a$$

This array can actually be achieved for surveys of small overall dimension when it is possible to put the distant electrodes some practical distance away. For a survey in an area of a few square meters “infinity” can be on the order of a hundred meters. Pole-pole sounding data is plotted as apparent resistivity vs. a.

b) <u>Pole-Dipole</u>

If only one of the current electrodes is placed at "infinity" the configuration and the apparent resistivity are as shown:

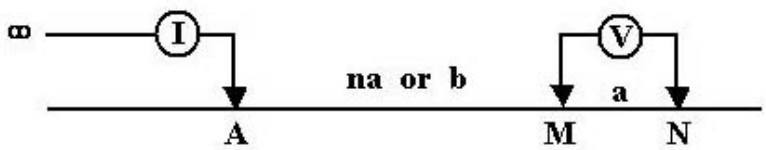

$$\rho_A = 2\pi \frac{b\,(a+b)}{a} \frac{V}{I}$$

This array is used frequently in resistivity surveying and the spacings are usually described, and taken, in integer multiples of the voltage electrode spacing b. The standard nomenclature is to call the potential electrode spacing a so the configuration and apparent resistivity become:

$$\rho_A = 2\pi \;\, a\; n\left(n+1\right) \frac{V}{I}.$$

Pole-dipole sounding data are plotted as apparent resistivity vs. a.

c) <u>Wenner</u>

The Wenner array is now seen to be a simple variant of the pole-dipole in which the distant pole at infinity is brought in and all the electrodes are given the same spacing, a, as seen in the following configuration

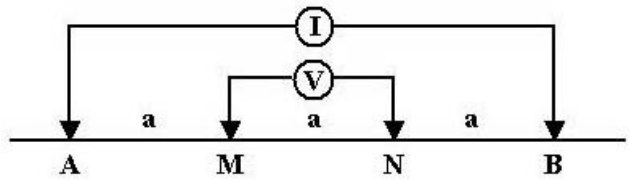

$$\rho_A = 2\pi\ a\,\frac{V}{I}$$

The Wenner array is normally used for sounding and the apparent resistivities are plotted vs. a on a log-log plot such as is shown in Figure 4.6.1. This data plot, for a Wenner sounding, can be qualitatively 'interpreted' by visual inspection. The shallow ground resistivity ~ 30 Ohm-m is revealed by the short spacing data; as the spacing increases the currents penetrate more deeply sensing a more resistive deeper layer.

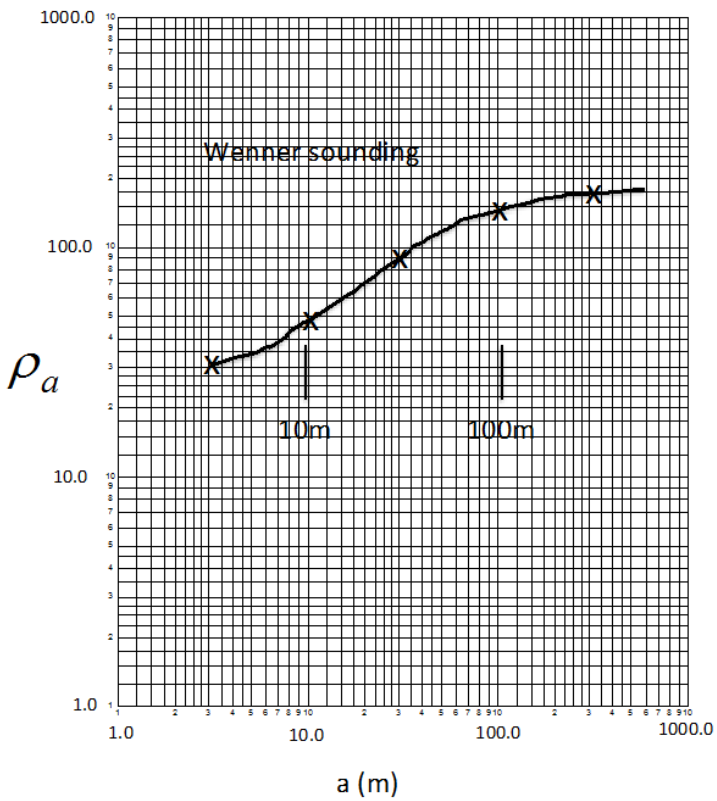

Figure 4.6.1

d) <u>Schlumberger</u>

One of the first arrays used in the 1920's and still popular today is the Schlumberger array shown below with its formula for apparent resistivity. It is another variant of the pole-dipole, again with the second current electrode placed symmetrically opposite the first. The voltage difference is consequently doubled and so the apparent resistivity is the same as that for the general pole-dipole with a factor of 1/2 in the geometric factor. In a Schlumberger sounding the voltage electrodes are usually kept small and fixed while only the b spacing is changed.

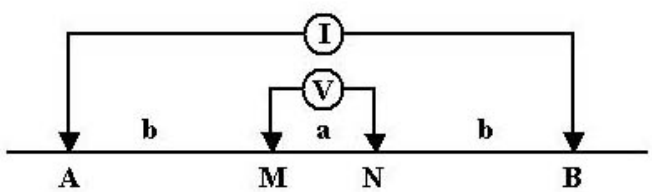

$$\rho_A = \frac{V}{I}\pi\frac{b\left(b+a\right)}{a} \approx \frac{V}{I}\pi\frac{b^2}{a} \qquad if \;\; a << b$$

[Note that if a is small compared to b, V/a ~ E the electric field. The electric field from an electrode is $-\partial\Phi/\partial r = I\rho/2\pi r^2$ and since there are two electrodes the total electric field becomes = $I\rho/\pi r^2$ and so $\rho_A = \frac{E}{I}\pi b^2$.]

Further, it is conventional to consider the spacing to be the distance from the center of the array to the outermost electrodes, i.e. AB/2. In this case b in the above

expressions becomes AB/2 – a/2. If a << AB/2 the above formulas for ρ_A are unchanged.

Data from a Schlumberger sounding is plotted vs. spacing in the same manner as the Wenner data. The structure of more complicated layered models is revealed directly from the apparent resistivity curves. The Schlumberger responses of several three- layer models are plotted in Figure 4.6.2.

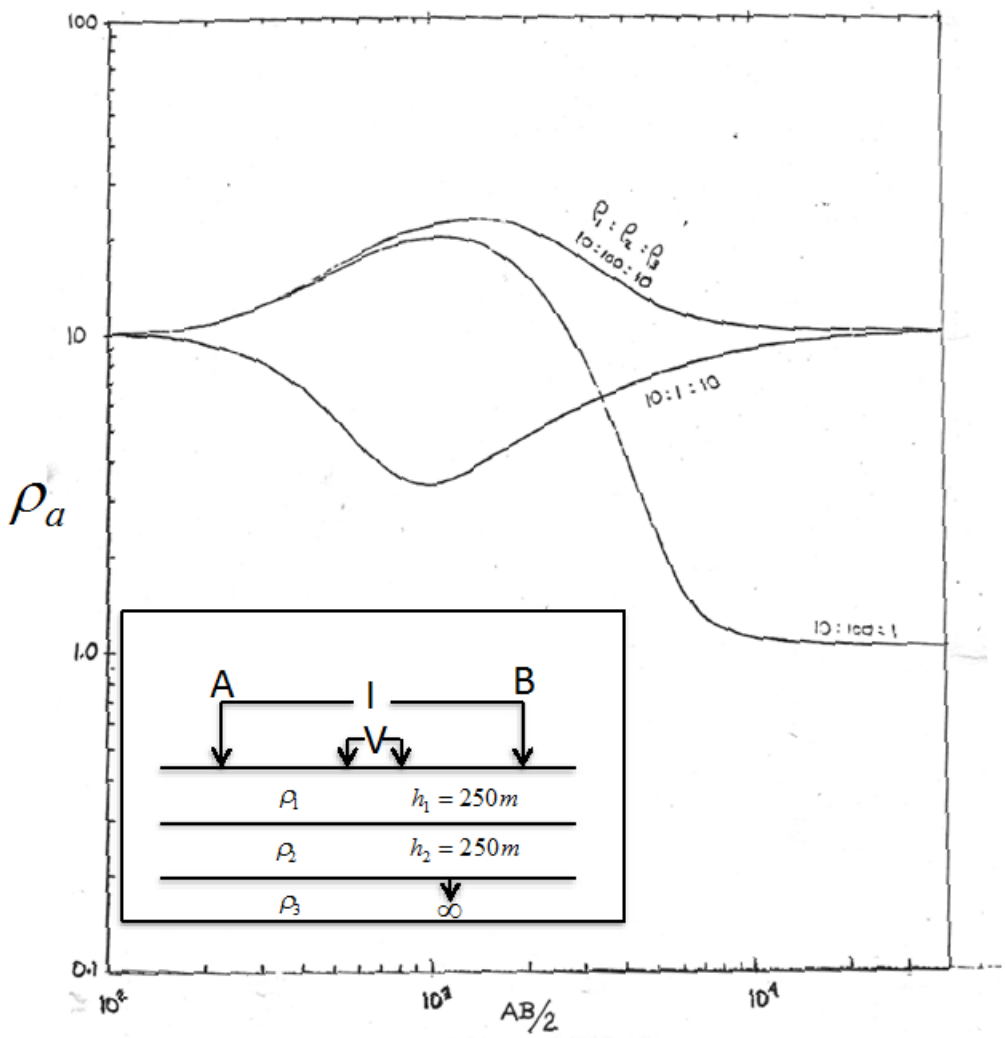

Figure 4.6.2

e) <u>Dipole-Dipole</u>

The dipole-dipole array is logistically the most convenient in the field, especially for large spacings. All the other arrays require significant lengths of wire to connect the power supply and voltmeter to their respective electrodes and these wires must be moved for every change in spacing as the array is either expanded for a sounding or moved along a line. For safety considerations alone it is not practical to lay out hundreds of meters of current carrying wire across terrain that may not be seen by the operator. The convention for the dipole-dipole array shown below is that current and voltage dipole spacing is the same, a, and the spacing between them is an integer multiple of a.

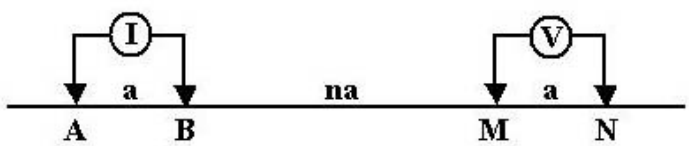

The apparent resistivity is given by:

$$\rho_A = \frac{V}{I} \pi \ a \ n(n+1)(n+2).$$

f) <u>Data plotting for the pole-pole, pole-dipole and dipole-dipole arrays</u>

The pole-pole, pole-dipole and dipole-dipole arrays are normally used in profiling mode to map lateral as well as depth variations in resistivity. The plotting convention is to plot the values of apparent resistivity at the intersection point of

two 45° lines descending from the current pole or dipole and from the voltage pole or dipole. This convention is illustrated for each of the arrays in Figure 4.6.3. The resulting "maps" of apparent resistivity are contoured at constant (usually logarithmic) intervals. The contoured sections are called "pseudo sections" because they look somewhat like resistivity cross-sections of the ground but they are not – they are simply a graphical representation of the data. The vertical scale is not depth but some function of the array spacing. For some geological models the pseudo sections do have an intuitive relationship to the actual section but mostly they do not. For a layered earth the contours are horizontal and rise and fall in value in the same sense as the actual resistivity, but for the case of a vertical contact between dissimilar resistivities the pseudo-section is a complex map with no direct relationship to the actual model. The example below shows dipole-dipole pseudo-sections for both layered earth and vertical contact models.

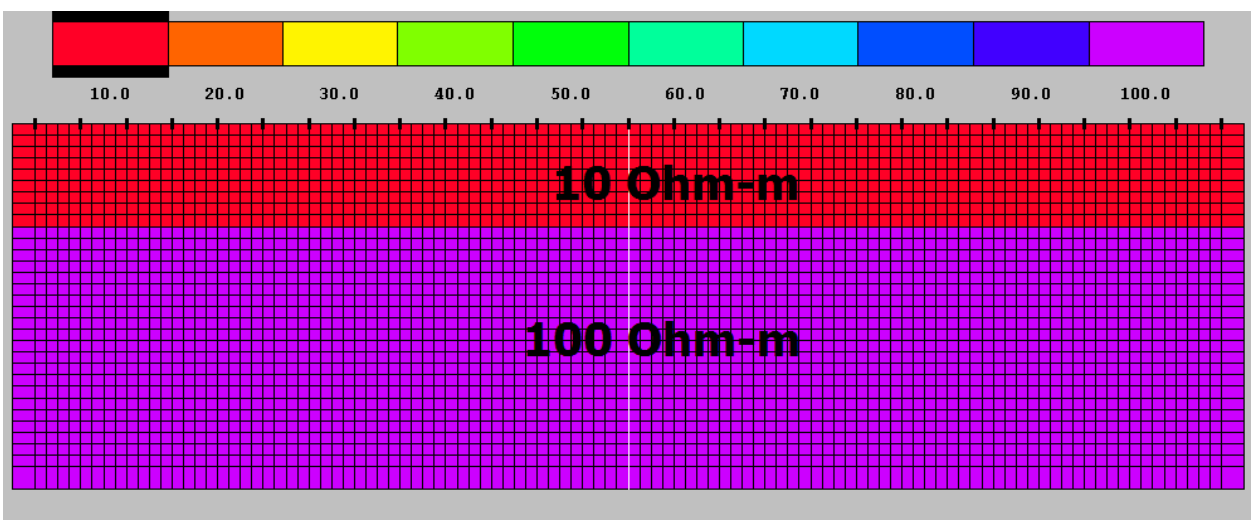

Two-layer model

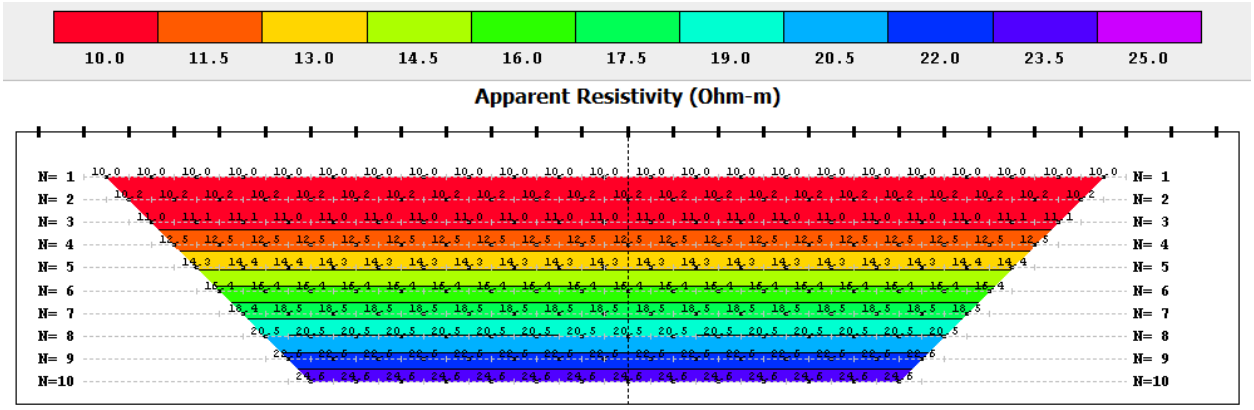

Figure 4.6.4a: Dipole-dipole pseudo-section of the two-layer model

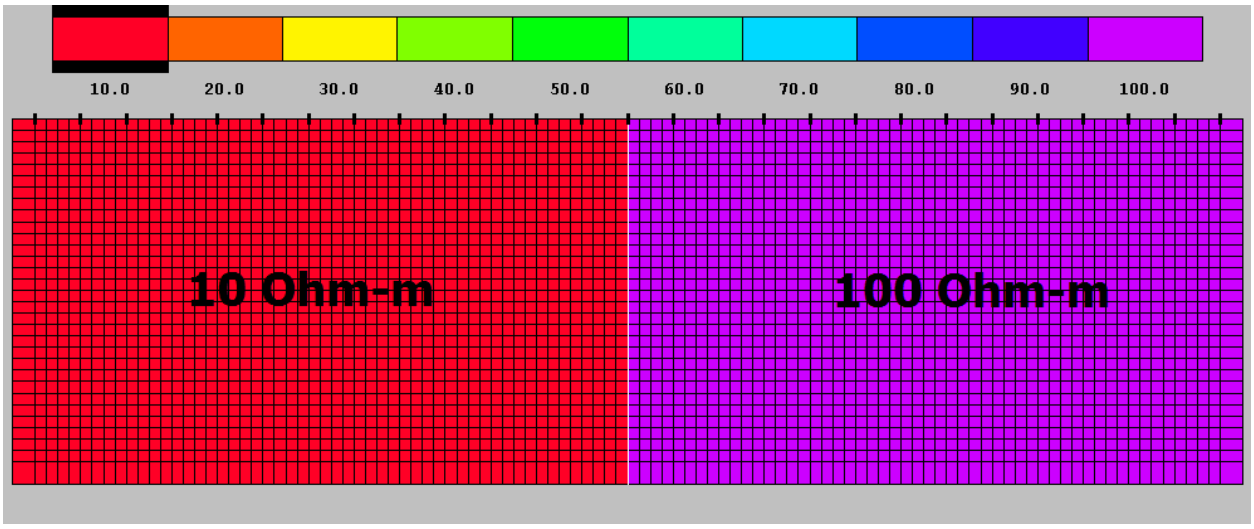

Vertical contact model

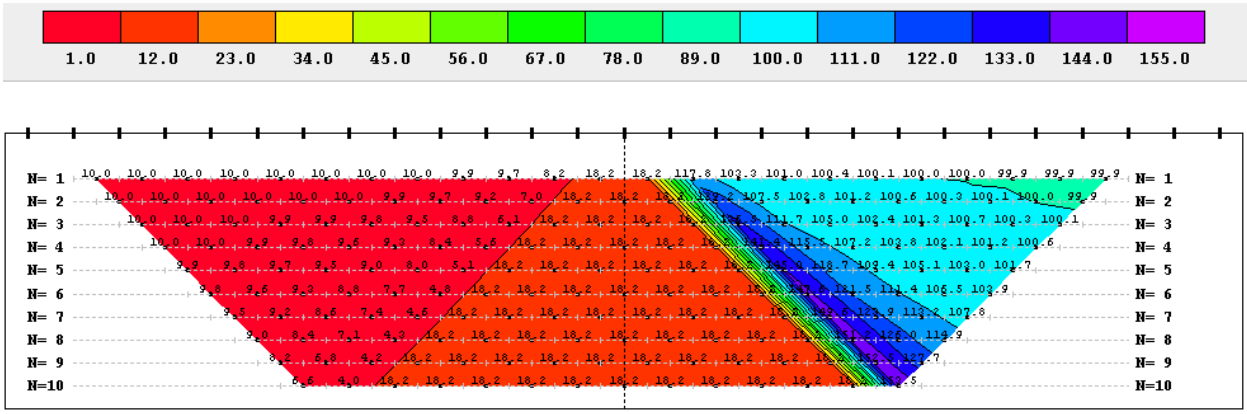

Figure 4.6.4b: Dipole-dipole pseudo-section of the vertical contact model

Return to top

Response of a layered Earth

a) Formal solution for current source on surface of uniform half space

The simple solution we derived in section 4.2 for a point source of current on the surface of a uniform half-space becomes more complicated if the current source is beneath the surface or if it is on the surface of, or within, a multi-layered medium. To set up the solutions for these models requires a slightly more formal approach to the boundary value problem.

From section 4.2 we found the equation of continuity to be:

$$\nabla \cdot J + \frac{\partial \varsigma}{\partial t} = 0 \qquad \text{where } \varsigma \text{ is the charge density.}$$

A physically plausible way for the charge density to increase in a region of space is to inject current, *I*, at point [actually in a tiny volume at a point in the medium]. In practice we inject this current with a wire leading from a power supply (e.g., battery) and there is assumed to be another point far away where the current is withdrawn.

We use the concept of a delta function to locate the point in space:

$$\nabla \cdot J = -\frac{\partial \varsigma}{\partial t}\delta\left(x - x^{'}\right)\delta\left(x - y^{'}\right)\delta\left(x - z^{'}\right)$$

for a point source of current at *x'*, *y'* and *y'*.

From our definitions of J, E. and conductivity, σ we can write:

$$\nabla \cdot \left(\sigma E\right) = \sigma \nabla \cdot \left(-\nabla \Phi\right) = -I\delta\left(x - x^{'}\right)\delta\left(x - y^{'}\right)\delta\left(x - z^{'}\right)$$

or, finally $$\nabla^2 \Phi = I\rho\delta\left(x - x^{'}\right)\delta\left(x - y^{'}\right)\delta\left(x - z^{'}\right)$$

This is Poisson's equation, and it is the starting point for DC electrical methods in applied geophysics.

In a homogeneous medium we found a solution for Φ when I is at the origin to be

$$\Phi(r) = \frac{I\rho}{4\pi r} \quad \text{where } r = \sqrt{x^2 + y^2 + z^2}$$

With the source on the surface of a uniform half space:

$$\Phi(r) = \frac{I\rho}{2\pi r}$$

<u>b) A point source of current near the contact between two half spaces</u>

A simple analytic result may be obtained for a buried source. Consider the source of current high to be located in medium 1 at a distance a from a plane interface between medium 1 and medium 2, as shown in the following sketch.

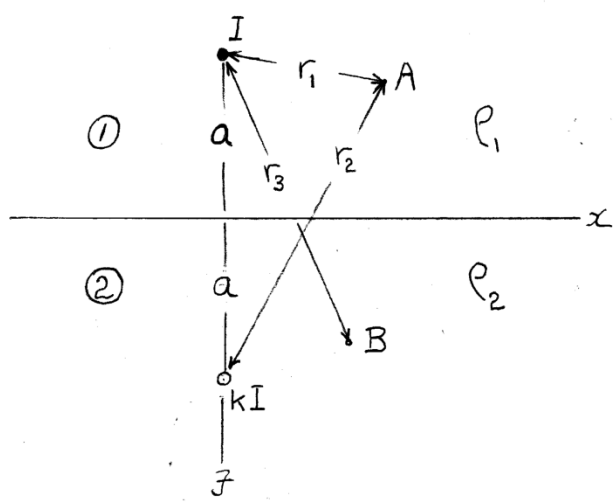

A fundamental aspect of any boundary value problem is that a solution to the governing partial differential equation that also satisfies the boundary conditions is *the* solution.

<u>The method of images</u>

By analogy with the image theory used in electrostatics we assume that the solution may be obtained by superimposing the fields from the actual source *I* with those of an image of source strength *kI* located at an equal distance on the other side of the contact.

In medium 1 assume that Φ at a point A, Φ_A, is given by:

$$\Phi_A = \frac{I\rho_1}{4\pi r_1} + \frac{kI\rho_1}{4\pi r_2}$$

And in medium 2 assume that:

$$\Phi_B = \frac{k' I\rho_2}{4\pi r_3}$$

These are all solutions to the governing Poisson equation and so now we have to see if they can be made to satisfy the boundary conditions:

1) Φ must be continuous across the boundary.

2) The normal current, $\frac{1}{\rho}\frac{\partial \Phi}{\partial z}$ must be continuous across the boundary.

Therefore, on the *z* axis, on the line joining *I* and *kI*.

$$\frac{I\rho_1}{4\pi a} + \frac{kI\rho_1}{4\pi a} = \frac{k' I\rho_2}{4\pi a} \quad \text{or} \quad \rho_1 + k\rho_1 = k'\rho_2$$

The normal current at *a* from each source is obtained from the operation

$$J = \frac{1}{\rho}(-\nabla\Phi\big|_{z=a})$$

And taking care with the signs of the derivatives to assure that the resulting currents are flowing in the right direction given the coordinate convention and location of the source, we find the currents at the interface along the line connecting the sources to be:

from I, $+\frac{I}{4\pi a^2}$, from kI $-\frac{kI}{4\pi a^2}$, and from $k'I$ $+\frac{k'I}{4\pi a^2}$

The boundary condition requires that the sum of the first two equals the third and this leads to:

$$1 - k = k'$$

Combining this with the condition on k from the potential boundary condition and solving for k yields:

$$k = \frac{\rho_2 - \rho_1}{\rho_2 + \rho_1}$$

and

$$k' = \frac{2\rho_1}{\rho_1 + \rho_2}$$

The hypothesis we started with an image current source can be made to satisfy the boundary conditions if the image current source in medium 2 seen from medium 1 has a magnitude of:

$$\frac{\rho_2 - \rho_1}{\rho_1 + \rho_2} \cdot I$$

With the k and k' known the field can be written anywhere from any source. For example if medium 2 is air then k goes to one and the fields on the interface are described by the sum of the source and its exact [equal amplitude] image on the other side in the air.

At a point at a radial distance R on the interface the potential would be:

$$\Phi_{R,z=0} = \frac{I\rho_1}{2\pi\sqrt{a^2 + R^2}}$$

c) The point source of current near a vertical contact

This same approach can be used for a point source on the surface of a half-space adjacent to a vertical contact separating two quarter spaces of resistivities ρ_1 and ρ_2. For this model the potential for the current sources are double the values for the potentials from sources in the whole space. This solution can be implemented for finding an analytic solution for the dipole-dipole apparent resistivity for a profile perpendicular to a vertical contact. This exact solution should be used to check the accuracy of numerical two-dimensional models.

We could continue with image theory from multiple layers but this approach is very cumbersome for many layers and so instead we turn to the general solution for a point source in or on the surface of a layered media.

d) Solution to Poisson's equation for a source of current on the surface of a layered media

The potentials from a point source of current on the surface of a horizontally layered media are functions only of the radial distance from the source and of the vertical rectangular coordinate *z*. It is therefore convenient to formulate Poisson's

equation in cylindrical coordinates. Expressing the Laplacian in cylindrical coordinates we find:

$$\frac{\partial^2\Phi}{\partial r^2}+\frac{1}{r}\frac{\partial\Phi}{\partial r}+\frac{\partial^2\Phi}{\partial z^2}=\frac{I\rho\delta(r)\delta(z-z')}{2\pi r}$$

[Note that the delta function for *r* in cylindrical coordinates is $\frac{\delta(r)}{2\pi r}$ because, by definition, the volume integral of a 3D delta function must be one. So in cylindrical coordinates, $\iiint\delta(r)\delta(\theta)\delta(z)r\,dr\,d\theta\,dz$ must be one.]

The solution could be derived by the classic method of separation of variables. Instead we choose to Fourier transform the z dependence and to use the Hankel transform on the *r* dependence.

We use the symmetric Hankel transform pair defined by:

$$\Phi(r)=\int_0^\infty\Phi(\lambda)J_0(\lambda r)\lambda\,d\lambda$$

and

$$\Phi(\lambda)=\int_0^\infty\Phi(r)J_0(\lambda r)r\,dr$$

we use the Fourier transform pair defined by:

$$\Phi(z)=\frac{1}{2\pi}\int_{-\infty}^{\infty}\Phi(k_z)e^{ik_z z}dk_z$$

$$\Phi(k_z)=\int_{-\infty}^{\infty}\Phi(z)e^{-ik_z z}dz$$

Note that in both transforms we have used the same symbol for the potential in both real and transform space. The parameters in brackets determine which is which.

If we now apply the transforms to the differential equation we obtain an algebraic equation in the transformed potentials viz;

$$-\lambda^2\Phi\left(\lambda,k_z\right)-k_z^2\Phi\left(\lambda,k_z\right)=\frac{I\rho}{2\pi}$$

so the solution in transform space is simply:

$$\Phi\left(\lambda,k_z\right)=-\frac{I\rho}{2\pi\left(\lambda^2+k_z^2\right)}$$

The solution back in *r*,*z* space is obtained by the inverse transform, namely:

$$\Phi\left(r,z\right)=-\frac{I\rho}{4\pi^2}\int_0^\infty\int_{-\infty}^\infty\frac{1}{\left(\lambda^2+k_z^2\right)}J_0\left(\lambda r\right)\lambda e^{ik_z z}dk_z d\lambda$$

First let's integrate this over k_z:

$$\Phi\left(r,z\right)=-\frac{I\rho}{4\pi^2}\int_{-\infty}^\infty\frac{e^{ik_z z}}{\left(\lambda^2+k_z^2\right)}dk_z=\frac{I\rho}{4\pi}\frac{e^{\pm\lambda z}}{\lambda}$$

Then integrate over λ back to *r* space:

$$\Phi\left(r,z\right)=\frac{I\rho}{4\pi}\int_0^\infty\frac{e^{-\lambda z}}{\lambda}J_0\left(\lambda r\right)\lambda d\lambda\quad=\frac{I\rho}{4\pi\sqrt{r^2+z^2}}$$

Which, rather comfortingly, is the answer we knew already from the simple whole space derivation earlier on.

We now have a very general method of solution which we can use to advantage for point sources on or within a layered medium. In the layered problem we are going to match boundary condition on planes where *z* is a constant, so we cannot work in k_z space.

However, the boundary conditions are independent of r so we can work in λ space. If we just transform the differential equation to λ space we are left with an ordinary differential equation in z that is quite simple to use. Starting with

$$-\lambda^2\Phi(\lambda,z)+\frac{d^2\Phi(\lambda,z)}{dz^2}=\frac{I\rho}{2\pi}$$

we have a solution in the medium with the source (called the primary field):

$$\Phi(\lambda,z)=\frac{I\rho}{4\pi}e^{\pm\lambda z}$$

where the sign must be chosen to make sure the potential falls off with increasing z. In regions not containing a source a solution to the homogeneous equation has the form:

$$\Phi(\lambda,z)=Ae^{\pm\lambda z}$$

To get a little practice with this approach, let's apply it to the problem where the source is located in medium 2, at the origin, and a boundary to medium 1 is located at $z=-z_1$. This is similar to the problem we solved earlier using the image method. The configuration is shown in the sketch below.

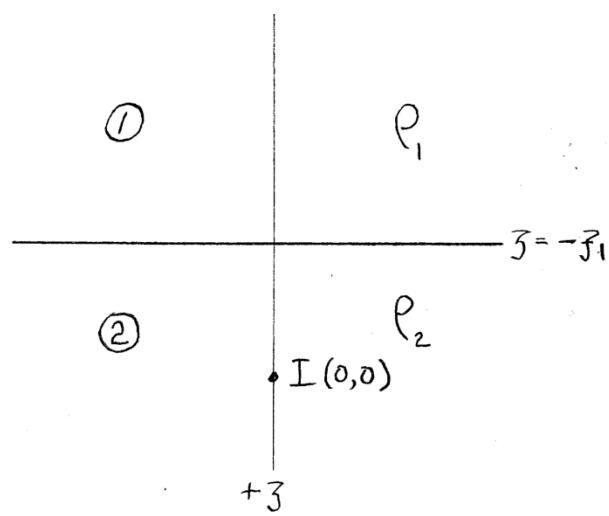

We assume that we can write the solution in medium 2 as the sum of the whole space solution for the source plus a secondary field caused by the boundary that satisfies the homogeneous equation. We assumed that the solution in medium 1 is a secondary field, again satisfying the homogeneous equation, that is caused by the boundary.

The primary field in medium 2 is given by:

$$\Phi(\lambda, z) = \frac{I\rho}{4\pi} e^{-\lambda z} \quad \text{if z >0}$$

$$\Phi(\lambda, z) = \frac{I\rho}{4\pi} e^{+\lambda z} \quad \text{if z<0}$$

The secondary fields in each medium have the form

$$\Phi(\lambda, z) = Ae^{\pm\lambda z}$$

Again, we must be very careful to select the correct sign so that the field falls off away from the boundary. This is very important because the boundary condition on the normal current involves the derivative of the potential evaluated at some value of *z*. The derivative must be taken first before setting the value of *z*. So in medium 1 the field must be $\Phi(\lambda, z) = A_1 e^{+\lambda z}$ for $z<-z_1$. But in the region between 0 and $-z_1$ the secondary field must grow as it approaches $-z_1$, so in medium 2 near the boundary $\Phi(\lambda, z) = A_1 e^{-\lambda z}$.

Applying the boundary condition that the potential must be continuous leads to:

$$\frac{I\rho}{4\pi}\frac{e^{+\lambda z_1}}{\lambda} + A_2 e^{-\lambda z_1} = A_1 e^{+\lambda z_1}$$

Applying the boundary condition that the normal current is continuous yields:

$$\frac{I\rho}{4\pi\rho_2}\frac{\lambda e^{+\lambda z_1}}{\lambda}-\frac{A_2\lambda e^{-\lambda z_1}}{\rho_2}=\frac{A_1\lambda e^{+\lambda z_1}}{\rho_1}$$

We have two equations in the two unknown coefficients A_1 and A_2. Solving for A_2 we find that:

$$A_2=\frac{\rho_1-\rho_2}{\rho_1-\rho_2}\cdot\frac{I\rho}{4\pi}\cdot\frac{e^{2\lambda z_1}}{\lambda}$$

The total potential in medium 2 is then given by:

$$\frac{I\rho}{4\pi}\cdot\frac{e^{\lambda z}}{\lambda}+\left[\frac{I\rho}{4\pi}\left(\frac{\rho_1-\rho_2}{\rho_1-\rho_2}\right)\frac{e^{2\lambda z_1}}{\lambda}\right]e^{-\lambda z}\qquad -z_1<z<0$$

This is the same result that we would have obtained if we had considered the boundary to have been replaced by another source at minus $-2z_1$ with a source strength multiplied by the factor $\left(\frac{\rho_1-\rho_2}{\rho_1-\rho_2}\right)$. This is where the original concept of the image source came from.

If medium 1 is air then $\left(\frac{\rho_1-\rho_2}{\rho_1-\rho_2}\right)$ is 1.0 and the potential in a half-space becomes:

$$\frac{I\rho}{4\pi}\cdot\frac{e^{\lambda z}}{\lambda}+\left[\frac{I\rho}{4\pi}\frac{e^{2\lambda z_1}}{\lambda}\right]e^{-\lambda z}\qquad -z_1<z<0$$

And finally, to close the loop, if z_1 goes to zero, i.e., the source goes to the boundary, then:

$$\Phi(\lambda,z)=\frac{I\rho}{2\pi}\frac{e^{-\lambda z}}{\lambda}$$

Back in r,z space

$$\Phi(r,z) = \frac{I\rho}{2\pi\sqrt{r^2+z^2}}$$

which, surprise, is the right answer for a source on the surface of the half-space.

Note in passing that in λ space the vertical current from this expression is $J_z = -\frac{1}{\rho}\frac{d\Phi}{dz} = \frac{I}{4\pi}e^{-\lambda z}$. The inverse Hankel transform of $e^{-\lambda z}$ has the form:

$$\int e^{-\lambda z} J_0(\lambda r)\lambda d\lambda = \frac{2z\Gamma\left(\frac{3}{2}\right)}{\sqrt{\pi\left(z^2+r^2\right)^{\frac{3}{2}}}}$$

(Gradshteyn and Ryzhik, 1965: formula 6.623)

which is zero evaluated at the air boundary, *z=0*.

With the formalism of solutions in λ, z space for point sources near a boundary firmly established, in numbing detail, we will now set up the solution to the multi-layer problem.

Consider trial solutions for a source is located at the surface of a two-layer model as shown in the sketch below.

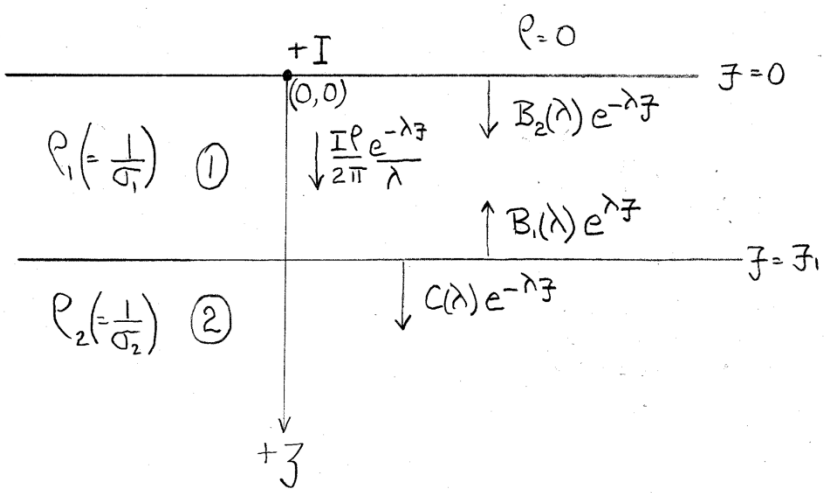

The assumed solutions use the point source solution for the half space with air above and the secondary potentials, that are solutions to the homogeneous equation, are caused by the boundaries at *z=0* and $z=z_1$.

The normal currents for the secondary fields are:

$$J_z = -\sigma_1 \frac{\delta \Phi^{\sec}}{\delta z} = -B_1 \sigma_1 \lambda e^{\lambda z} + B_2 \sigma_1 \lambda e^{-\lambda z}$$

But at *z=0* the current must be zero so $B_1 \sigma_1 \lambda = B_2 \sigma_1 \lambda$ *i.e.*, $B_2 = B_1$.

The secondary potential due to the boundaries is therefore;

$$\Phi^{\sec} = B_1 (e^{\lambda z} - e^{-\lambda z})$$

The total potential in layer 1 is then:

$$\Phi = \frac{I\rho}{2\pi} \frac{e^{-\lambda z}}{\lambda} + B_1 (e^{\lambda z} - e^{-\lambda z})$$

In medium 2 the potential is $C(\lambda) e^{-\lambda z}$ and the normal current is $J_z = C \sigma_2 \lambda e^{-\lambda z}$.

For any medium we now introduce the characteristic impedance defined as:

$$\eta = \frac{\Phi(\lambda, z)}{J_z(\lambda, z)} = \frac{1}{\sigma \lambda}.$$

For algebraic simplicity in the following development we define

$$A(\lambda) = \frac{I\rho}{2\pi\lambda} = \frac{I}{2\pi\sigma\lambda}$$

The ratio of the total potential to the normal current at $z=z_1$ we define as the surface impedance of medium 2, and it is:

$$Z_2 = \frac{\Phi^{z_1}}{J_z^{z_1}} = \frac{Ae^{-\lambda z_1} + B\left(e^{\lambda z_1} + e^{-\lambda z_1}\right)}{\frac{Ae^{-\lambda z_1}}{\eta_1} + \frac{B}{\eta_1}(e^{\lambda z_1} + e^{-\lambda z_1})} = \frac{Ce^{-\lambda z_1}}{\frac{C}{\eta_2}e^{-\lambda z_1}} = \eta_2$$

With a bit of tedious algebra we can find the solution for *B:*

$$B = \frac{Ae^{-\lambda z_1}\left(Z_2 - \eta_1\right)}{\eta_1\left(e^{\lambda z_i} + e^{-\lambda z_i}\right) - Z_2\left(e^{-\lambda z_i} - e^{\lambda z_i}\right)}$$

and so the expression for the potential in layer 1 becomes:

$$\begin{aligned}\Phi &= Ae^{-\lambda z} + B(e^{\lambda z} - e^{-\lambda z}) \\ &= Ae^{-\lambda z} + \frac{Ae^{-\lambda z_1}\left(Z_2 - \eta_1\right)}{\eta_1\left(e^{\lambda z_i} + e^{-\lambda z_i}\right) - Z_2\left(e^{-\lambda z_i} - e^{\lambda z_i}\right)}\left(e^{\lambda z} + e^{-\lambda z}\right)\end{aligned}$$

And with a little rearranging and setting z to zero we have for the potential on the surface of the half-space:

$$\Phi\left(\lambda, z=0\right) = A \cdot \frac{\eta_1\left(e^{\lambda z_1} - e^{-\lambda z_1}\right) + Z_2\left(e^{\lambda z_1} + e^{-\lambda z_1}\right)}{\eta_1\left(e^{\lambda z_1} + e^{-\lambda z_1}\right) + Z_2\left(e^{\lambda z_1} - e^{-\lambda z_1}\right)}$$

Dividing top and bottom by $\left(e^{\lambda z_1} + e^{-\lambda z_1}\right)$ we arrive finally at the expression for the surface potential:

$$\begin{aligned}\Phi_i &= a_i e^{-\lambda z_{i-1}} + b_i e^{\lambda z_{i-1}} \\ J_i &= \frac{a_i e^{-\lambda z_{i-1}}}{\eta_i} - \frac{b_i e^{\lambda z_{i-1}}}{\eta_i}\end{aligned}$$

$$\Phi\left(\lambda, z=0\right) = A(\lambda) \cdot \left(\frac{\eta_1 \tanh\left(\lambda z_1\right) + Z_2}{\eta_1 + Z_2 \tanh\left(\lambda z_1\right)}\right)$$

This elegant solution shows that the effect of the surface layer simply modifies the simple half-space solution $A(\lambda)\left(=\dfrac{I}{2\pi\lambda\sigma_1}\right)$ for a medium of the first layer conductivity by a factor that depends on the thickness of the layer, the characteristic impedance of the layer and the surface impedance of the next layer down. For this simple model the next layer down is in fact a half-space and so its surface impedance is its characteristic impedance. But the solution is the same if in fact we find an expression for the surface impedance on top of a whole series of layers.

For an n-layer model shown in the sketch below we will now find a general recursion relationship for the surface impedance at the top of a layer to the surface impedance at the bottom of the layer or the top of the next layer down which is the same thing.

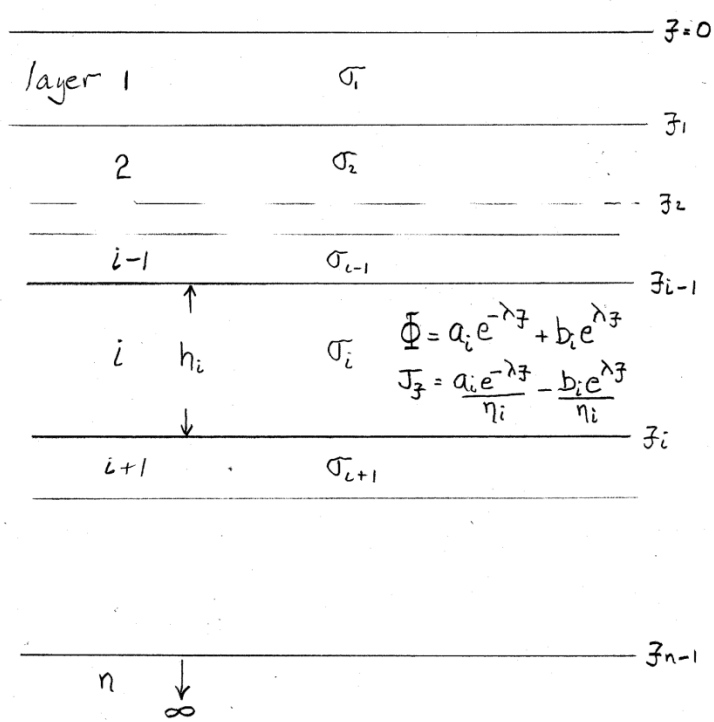

The solutions for the potential and normal current in layer i are shown in the sketch. A similar solution set exists for the layer above and below except with layer subscripts i-1 and i+1 respectively. The solutions have to match at $z=z_i$ so the solutions in layer i and layer $i+1$ *evaluated at* $z=z_i$ have to be equal:

$$\Phi_i\Big|_{z=z_i} = a_{i+1}e^{-\lambda z_i} + b_{i+1}e^{\lambda z_i} \qquad \Phi_{i+1}\Big|_{z=z_i} = a_i e^{-\lambda z_i} + b_i e^{\lambda z_i}$$

$$J_i\Big|_{z=z_i} = \frac{a_{i+1}e^{-\lambda z_i}}{\eta_{i+1}} - \frac{b_{i+1}e^{\lambda z_i}}{\eta_{i+1}} \quad \text{and} \quad J_{i+1}\Big|_{z=z_i} = \frac{a_i e^{-\lambda z_i}}{\eta_{i+1}} - \frac{b_i e^{\lambda z_i}}{\eta_{i+1}}$$

this means that we can express the coefficients in layer I in terms of the potential and normal current at the top of the layer below, i.e. in matrix form:

$$\begin{vmatrix} \Phi_{i+1} \\ J_{i+1} \end{vmatrix}_{z=z_i} = |B| \cdot \begin{vmatrix} a_i \\ b_i \end{vmatrix} \qquad \text{where} \qquad |B| = \begin{vmatrix} e^{-\lambda z_i} & e^{\lambda z_i} \\ \dfrac{e^{-\lambda z_i}}{\eta_i} & -\dfrac{e^{\lambda z_i}}{\eta_i} \end{vmatrix}$$

from which we can express a_i and b_i via

$$\begin{vmatrix} a_i \\ b_i \end{vmatrix} = |B|^{-1} \cdot \begin{vmatrix} \Phi_{i+1} \\ J_{i+1} \end{vmatrix}_{z=z_i}$$

In the layer above at the interface where the solutions are continuous we can write the solutions at $z=z_{i-1}$ as:

$$\Phi_i = a_i e^{-\lambda z_{i-1}} + b_i e^{\lambda z_{i-1}}$$

$$J_i = \frac{a_i e^{-\lambda z_{i-1}}}{\eta_i} - \frac{b_i e^{\lambda z_{i-1}}}{\eta_i}$$

or again in matrix form as

$$\begin{vmatrix} \Phi_i \\ J_i \end{vmatrix}_{z=z_{i-1}} = |A| \cdot \begin{vmatrix} a_i \\ b_i \end{vmatrix} \qquad \text{where} \qquad |A| = \begin{vmatrix} e^{-\lambda z_{i-1}} & e^{\lambda z_{i-1}} \\ \dfrac{e^{-\lambda z_{i-1}}}{\eta_i} & -\dfrac{e^{\lambda z_{i-1}}}{\eta_i} \end{vmatrix}$$

but we already have a matrix relating a_i and b_i to the potential and normal current at z_i so we can combine these equations to yield:

$$\left|\begin{matrix}\Phi_i \\ J_i\end{matrix}\right|_{z=z_{i-1}} = |A| \cdot |B|^{-1} \cdot \left|\begin{matrix}\Phi_{i+1} \\ J_{i+1}\end{matrix}\right|_{z=z_i}$$

The inverse of matrix B is;

$$|B|^{-1} = -\frac{\eta_i}{2} \cdot \left|\begin{matrix} -\dfrac{e^{-\lambda z_i}}{\eta_i} & -e^{\lambda z_i} \\ \dfrac{e^{-\lambda z_i}}{\eta_i} & +e^{\lambda z_i} \end{matrix}\right|$$

so multiplying out

$$|A| \cdot |B|^{-1} = \frac{-\eta_i}{2} \left|\begin{matrix} -\dfrac{1}{\eta_i}\left(e^{\lambda h_i} + e^{-\lambda h_i}\right) & -\left(e^{\lambda h_i} - e^{-\lambda h_i}\right) \\ -\dfrac{1}{\eta_i^2}\left(e^{\lambda h_i} - e^{-\lambda h_i}\right) & -\dfrac{1}{\eta_i}\left(e^{\lambda z_i} + e^{-\lambda z_i}\right) \end{matrix}\right|$$

In the multiplication of the exponential terms we have used the fact that $z_i - z_{i-1} = h_i$. If we expand this matrix equation into two equations for the potential and normal current and divide one by the other we get:

$$\left.\frac{\Phi_i}{J_i}\right|_{z=z_{i-1}} = \frac{\dfrac{1}{\eta_i}\left(e^{\lambda h_i} + e^{-\lambda h_i}\right)\Phi_{i+1} + \left(e^{\lambda h_i} - e^{-\lambda h_i}\right)J_{i+1}}{\dfrac{1}{\eta_i^2}\left(e^{\lambda h_i} - e^{-\lambda h_i}\right)\Phi_{i+1} + \dfrac{1}{\eta_i}\left(e^{\lambda h_i} + e^{-\lambda h_i}\right)J_{i+1}}$$

Now divide the top and bottom of the right hand side by $\left(e^{\lambda h_i} + e^{-\lambda h_i}\right)$ and noting that $\dfrac{\Phi_{i+1}}{J_{i+1}} = Z_{i+1}$, the surface impedance at the top of layer *i+1*, we find the simple recurrence formula that expresses the surface impedance of a layer in terms of the surface impedance of the layer below.

$$Z_i = \eta_i \cdot \frac{\eta_i \tanh\left(\lambda h_i\right) + Z_{i+1}}{\eta_i + Z_{i+1} \tanh\left(\lambda h_i\right)}$$

An interesting observation is that when we solved for the model in which a current source was placed on the surface of a two layer model we found the solution for the potential on the surface to be:

$$\Phi\left(\lambda, z = 0\right) = \frac{I}{2\pi\sigma_1\lambda} \cdot \left(\frac{\eta_1 \tanh\left(\lambda z_1\right) + Z_2}{\eta_1 + Z_2 \tanh\left(\lambda z_1\right)}\right)$$

Dividing both sides by $\frac{I}{2\pi}$,

$$\frac{2\pi\,\Phi\left(\lambda, z = 0\right)}{I} = \eta_1 \cdot \left(\frac{\eta_1 \tanh\left(\lambda z_1\right) + Z_2}{\eta_1 + Z_2 \tanh\left(\lambda z_1\right)}\right)$$

This is exactly the form of the solution for Z at the top of any layer in the above n-layer derivation but in this case the surface impedance at the earth-air boundary has rather special meaning, it *is the potential divided by the injected current rather than the normal current that flows across boundaries of differing finite resistivity.* In any event we now have the formula for finding the potential on the surface, in λ space, for a layered half-space and any injected current a distance of r away on the surface. The interactive window for this section uses this approach to find the potential for a point source of current. The integration from λ space to particular values of r is done numerically. This whole approach is easily generalized to find the potentials within any layer and to find them if the source is located within a layer.

e) A multi-layer numerical modeling code for apparent resistivity: **1-D Resistivity**

The formulation developed above has been programmed to produce plots of apparent resistivity for n-layered models of arbitrary layer thickness and resistivity and is available as **1-D Resistivity** in the included Java applets.

f) The Particular Case of the 2-layer model

A schematic generic two-layer model with for both Wenner and Schlumberger arrays is shown in Figure 4.6.5.

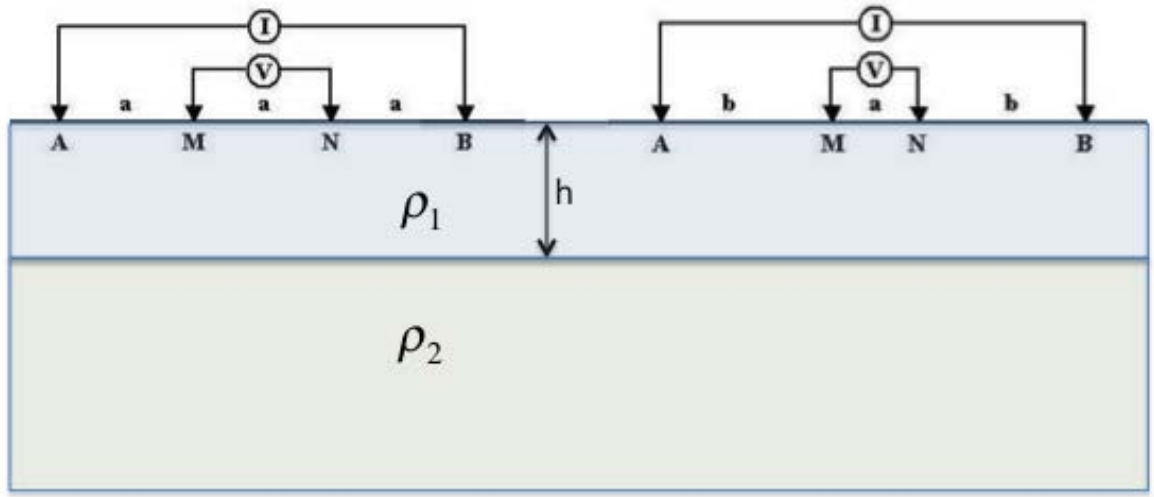

Figure 4.6.5

It can be seen in the theoretical formulation that the apparent resistivity and the spacing can be normalized by the first layer resistivity and the first layer thickness

respectively. This permits a family of model results for varying second layer resistivity to be plotted on the same graph as is shown in Figure 4.6.6.

The spacing scales are different; the Wenner spacing *a* normalized by the layer thickness h is on the top margin of the plot, the Schlumberger spacing normalized by the thickness h is on the bottom. The left axis is the value of the observed or calculated apparent resistivity normalized by the first layer resistivity ρ_1. On the right the response curves are labeled with the ratio of the second ρ_2 to first, ρ_1, layer resistivities.

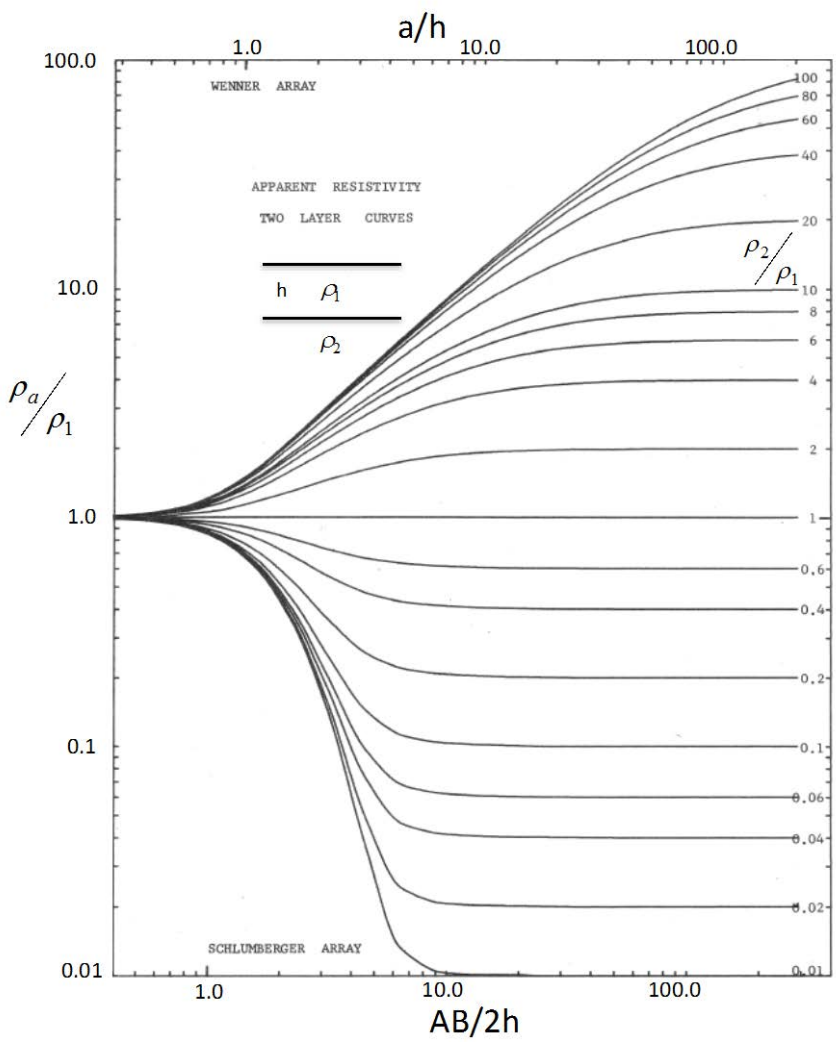

Figure 4.6.6

These simple two layer master curves, and an example of three-layer curves of Figure 4.6.2 (repeated below) illustrate several important features of resistivity soundings:

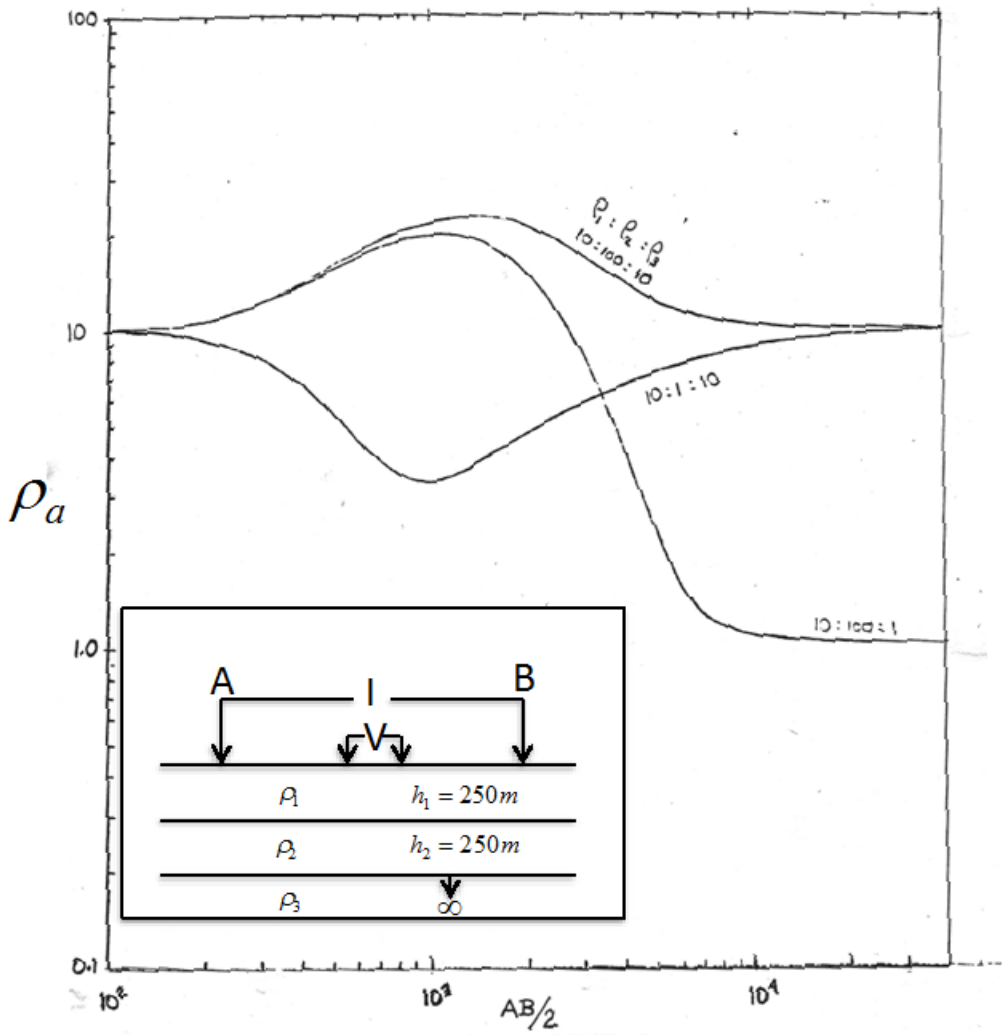

Figure 4.6.2

i. Soundings are not symmetrical for resistive or conductive basement. The master curves clearly show that the apparent resistivity asymptotes to the resistivity of a conductive basement at much smaller spacings than for a resistive one. This sensitivity to conductive layers is also evident in the

three-layer model where a layer of 10 times the first layer resistivity shows a maximum apparent resistivity of about 2.25 times the first layer resistivity whereas a conductive layer of one tenth the first layer resistivity causes a decrease of apparent resistivity to about one third of the first layer resistivity. This asymmetry disappears when the second layer is thin compared to the first layer.

ii. *Detecting* layers in a sounding requires relative modest spacings. From the two-layer model curves it is seen that a resistive or conductive second layer is revealed with spacings of one or two times the layer thickness h. To properly identify the lower layer resistivity would require spacings out to 10 or 20 times h for a resistive basement but only to 6 or 7 times h for a conductive basement.

iii. *Defining* the layer parameters requires far greater spacings. The three layer curves show that to define the layer parameter in a model fitting would require spacings of out to at least 25 times the first layer thickness, or for the large scale model used in Figure 4.6.2, spacing of 6000 meters. Noting that this spacing is half the overall current electrode spacing, this means that to resolve layering down to 500 m an electrode array on the surface of length 12 km would be required. To simply detect a conductive basement would only require an array of about 2-3 km length.

These ‘master’ curves can readily be used to interpret field results that suggest a simple two layer geology. As an example the field data used to illustrate the plotting convention for a Wenner sounding in Figure 4.6.1 is plotted in red in

Figure 4.6.7 on the two-layer master curves having been shifted horizontally and vertically to 'match' one of the master curves in Figure 4.6.6.

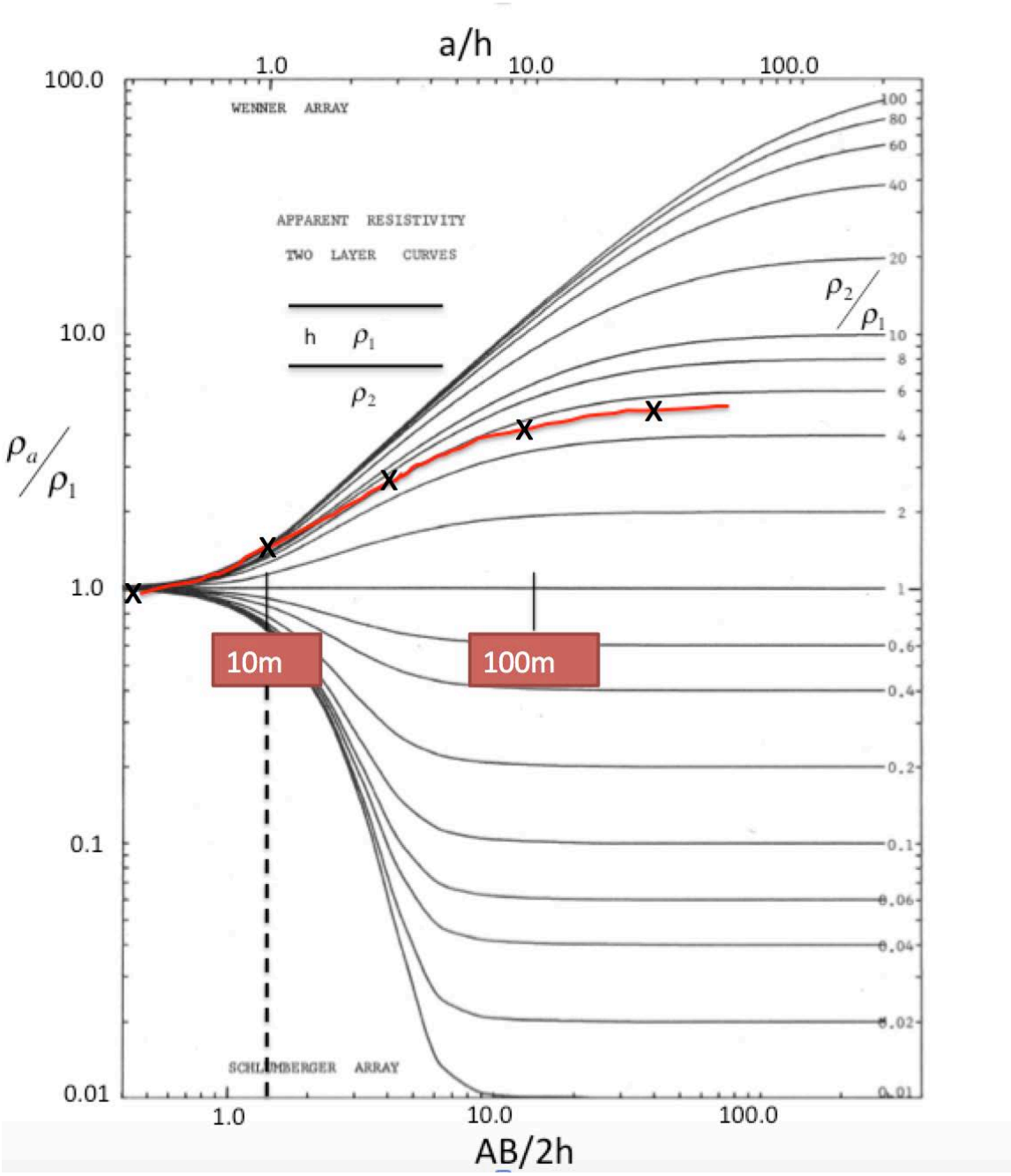

Figure 4.6.7

From the field data plot it is evident that the first layer resistivity is about 30 Ohm-m. The curve match indicates the second layer is about 5 times ρ_1 or 150 Ohm-m and the spacing scale shows a match of a/h equal to one when *a* is 10 so the layer thickness is 10 m.

Return to top

The impact of small scale near surface inhomogeneities

The very large spacings needed in Wenner and Schlumberger resistivity soundings, up to 20 times the depth of investigation, require geological settings with a very uniform lateral distribution of resistivity. Lateral changes in the surface layer exert a major effect on the apparent resistivities observed in a sounding as the electrodes move over them as the array expands resulting in sometimes 'jagged' variations in the apparent resistivity curves prohibiting the fitting of a smooth layered model curve. In a Schlumberger sounding, if the fixed potential electrodes happen to be in an unrecognized near surface 'patch' of conductive material the entire sounding curve will be shifted down.

A field example where these effects are seen is in the Wenner sounding of Figure 4.6.8. The closely spaced variations in the response curve cannot be caused by horizontally uniform variations in the vertical resistivity distribution, so the best fit three-layer model (thicknesses and resistivities shown in the model parameter box in the lower left corner) may or may not represent an actual layered geology.

If near surface variations are suspected it is necessary to use multiple soundings, the center of each of which is shifted along a survey by distances on the order of

the expected lateral resistivity dimensions. This turns out to be impractical because the deployment of the cable layouts for each sounding repeated over and over along the survey line is too time consuming.

Wenner resistivity sounding: Richmond Field Station

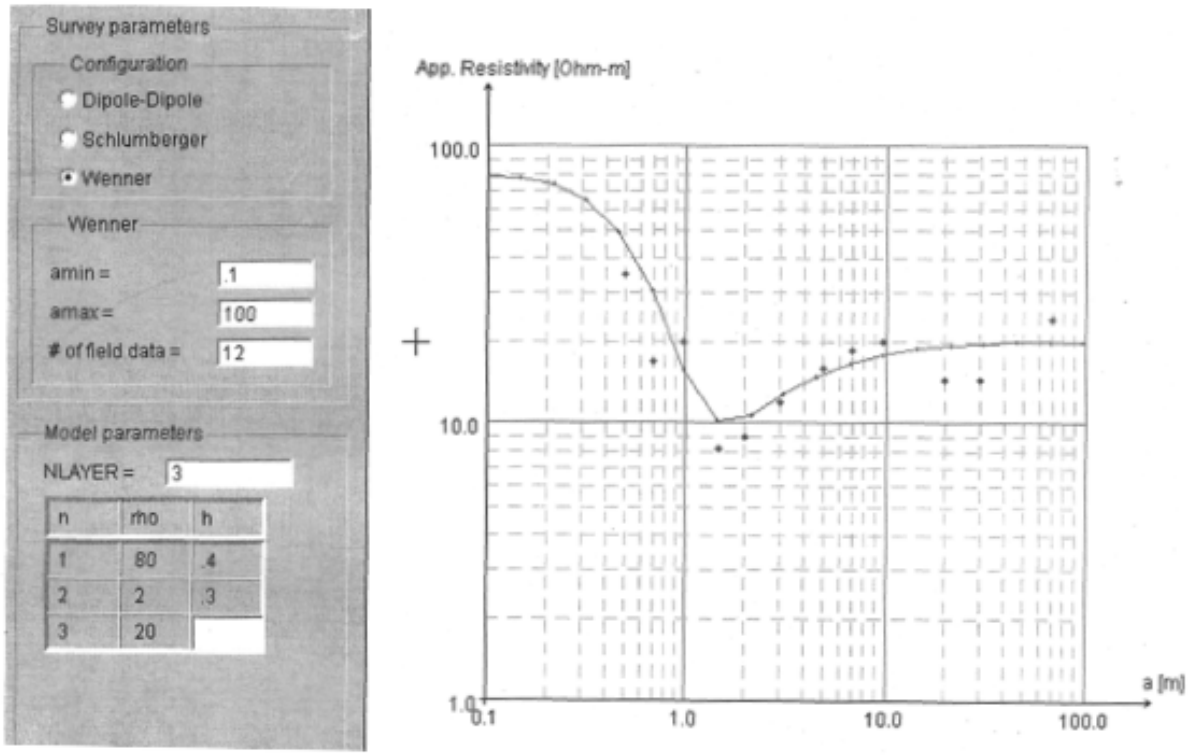

Three-layer inversion

Figure 4.6.8

The best solution for this problem is to use the dipole-dipole array. The dipole-dipole array inherently combines a traversing and sounding measurement. As discussed above the dipole-dipole array is also the most convenient in the field logistically, especially for large spacings. All the other arrays require significant lengths of wire to connect the power supply and voltmeter to their respective

electrodes and these wires must be moved for every change in spacing as the array is either expanded for a sounding or moved along a line in a traverse. The dipole-dipole array provides the best resolution both laterally and vertically that is achievable with the most efficient and safe field layout of electrodes and their associated cables.

A dipole-dipole survey was conducted on a line in the vicinity of the sounding shown in Figure 4.6.8. This survey was conducted with 1.0 m dipoles to reveal detail resistivity variations in the near surface. The dipole-dipole pseudo sections were inverted to produce the 'true' two-dimensional resistivity section of Figure 4.6.9.

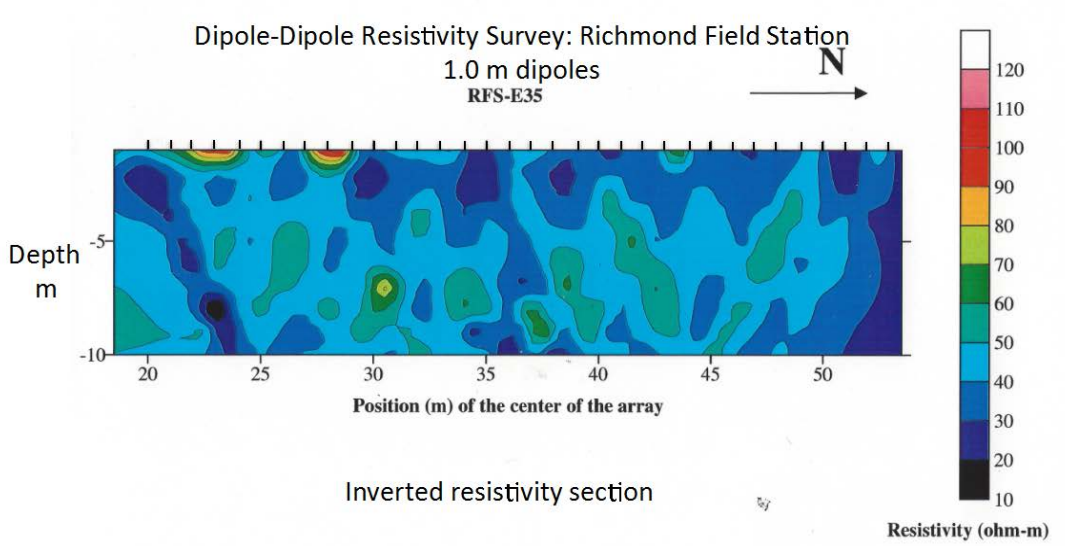

Figure 4.6.9

As suspected the near surface is highly inhomogeneous with small regions of resistivity varying from 10 to almost 100 Ohm-m. A single sounding anywhere along the profile could not be expected to yield a reliable equivalent layer model for this site. [The near surface at this site is made up of landfill from different sources and consists of mixed clays (conductive) and sand-gravels (resistive).

Resolution of the expected layered alluvial sands and clays beneath this surface layer would require a larger scale dipole- dipole survey using 10 or 30 m dipoles with n values up to 10 or 15, but these would be still 'contaminated' by the near surface features.]

Return to top

Detection and resolution of thin layers

The depth to which a particular resistivity array can detect and characterize a thin layer is often used as a measure of the *depth of exploration* for that array. A thin layer depth section is shown with a Schlumberger array in Figure 4.6.10.

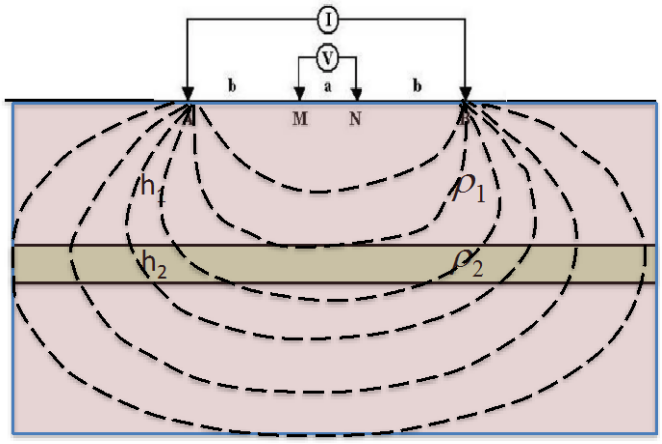

Figure 4.6.10

Thin in this context is $h_2 << h_1$. The resistivities of the thin layer can be greater or less than the resistivity of the enclosing half space. The current flow lines shown are approximately those that would occur in a uniform half space. It might be expected from a consideration of the current flow lines that a thin resistor would block vertical current flow, with some shunting of horizontal current flow directly beneath the bipole, and would have a major effect on the apparent resistivity. A

thin conductor would have very little effect on the vertical currents and would not perturb the apparent resistivity appreciably. In fact, accurate numerical modeling of the Schlumberger response of resistive and conductive layers shows a comparable effect, as seen in Figure 4.6.11. Here, the background resistivity is 100 Ohm-m, with the layer resistivity either 10 or 1000 Ohm-m. Each layer causes ~13% response change. This is unlike the asymmetric response observed for resistive and conductive basements in the two-layer curves of Figure 4.6.5.

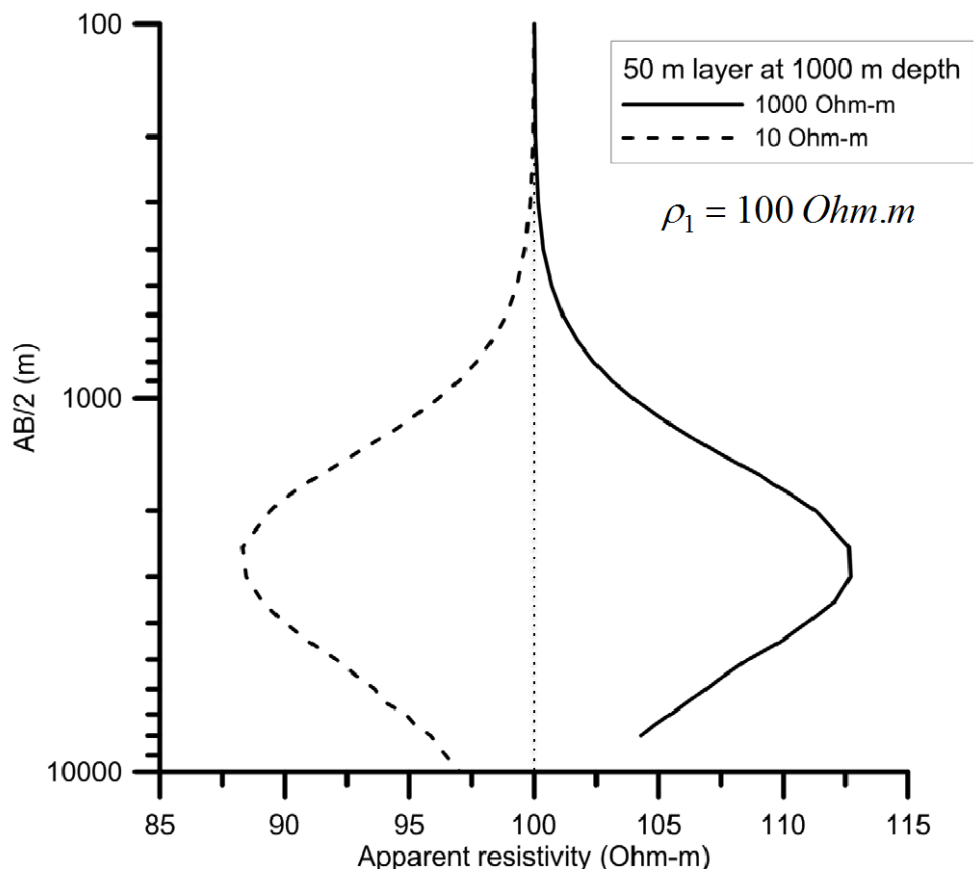

Figure 4.6.11

An important observation from modeling the response of thin layers is that the response of a thin resistive layer only depends on the product of the resistivity and the layer thickness: for a conductive layer it depends only on the product of the

conductivity and the thickness. This obviously precludes the determination of the value of the actual layer thickness or either the conductivity or resistivity from surface measurements. [Note that if the thickness were reliably determined from seismic measurements, the resistivity could be determined leading for example to an estimate of oil saturation.]

Return to top

The anisotropic half-space

A lower sensitivity to horizontal thin resistors is a manifestation of a fundamental property of the response of vertically anisotropic half-spaces. Keller [1966] showed that for an anisotropic half-space characterized by a vertical or transverse resistivity ρ_t and longitudinal or horizontal resistivity ρ_l (the coefficient of anisotropy is defined as $\lambda = \sqrt{\frac{\rho_t}{\rho_l}}$), the apparent resistivity for a surface-based array is given by $\rho_a = \lambda \rho_l$ or $\sqrt{\rho_t \rho_l}$. On a macroscopic scale, an alternating sequence of equal thickness layers of 100 and 10 Ohm-m has a transverse resistivity of 55 Ohm-m and a longitudinal resistivity of 18.2 Ohm-m. The transverse resistivity is biased towards the resistive layer while the longitudinal resistivity is biased towards the low resistivity layer. Current flow from a surface electrode is impeded by resistive layers, but longitudinal flow in conductive layers reduces the blocking effect. For the alternating sequence above,

the apparent resistivity for a surface array would be 31.6 Ohm-m., closer to the longitudinal resistivity than to the transverse. These results are even more counter-intuitive for vertical electrode arrays in a borehole, where *the measured apparent resistivity is the longitudinal resistivity.* The current flow is most strongly influenced by the conductive layers in the section. This phenomenon is referred to as the paradox of anisotropy. The important conclusion is that in a generally conductive section surface and borehole DC resistivity techniques are relatively insensitive to flat lying resistive layers.

A confirmation of these results is shown in the two-dimensional model of banded 10 and 100 Ohm-m horizontal and vertical layers shown in Figures 4.6.12a and 4.6.12b below.

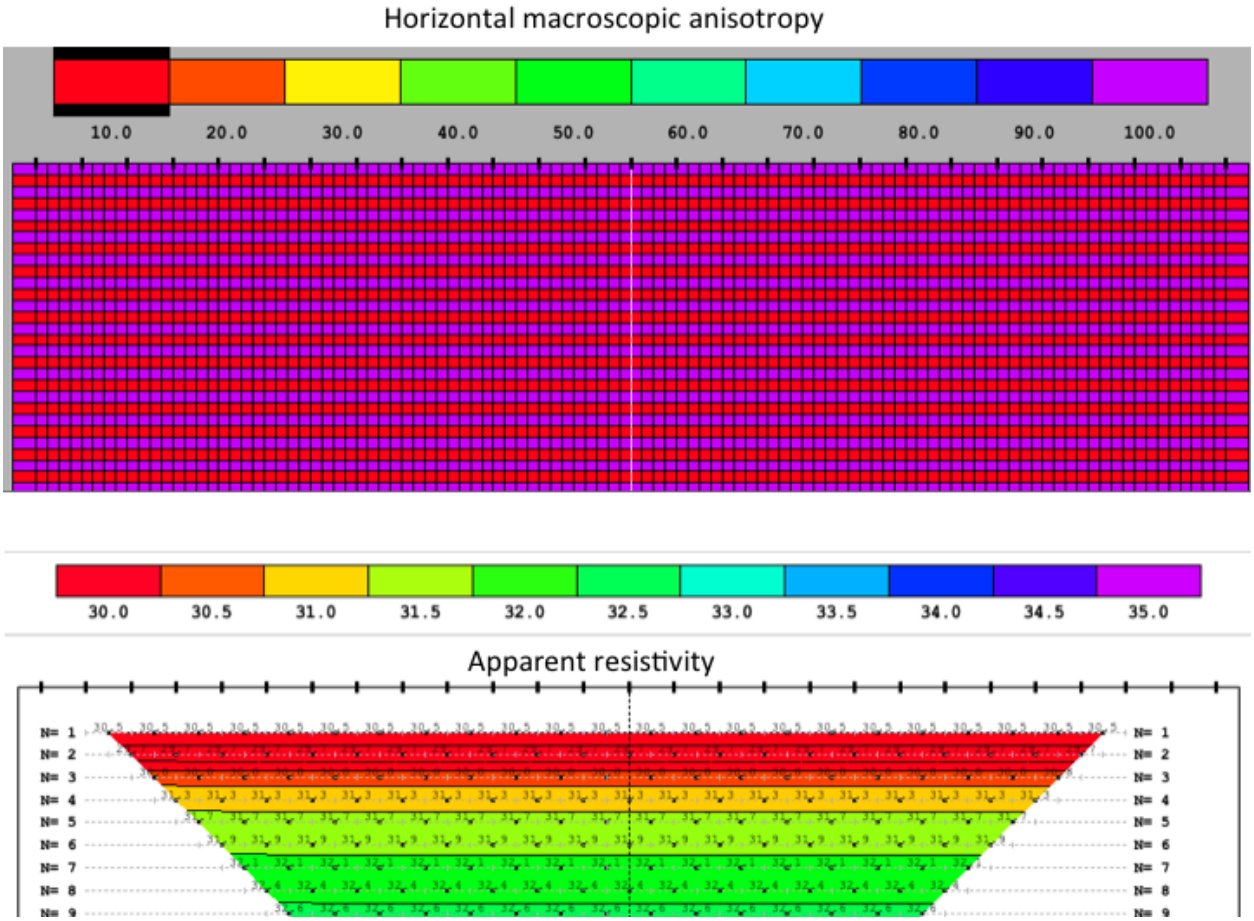

Figure 4.6.12a

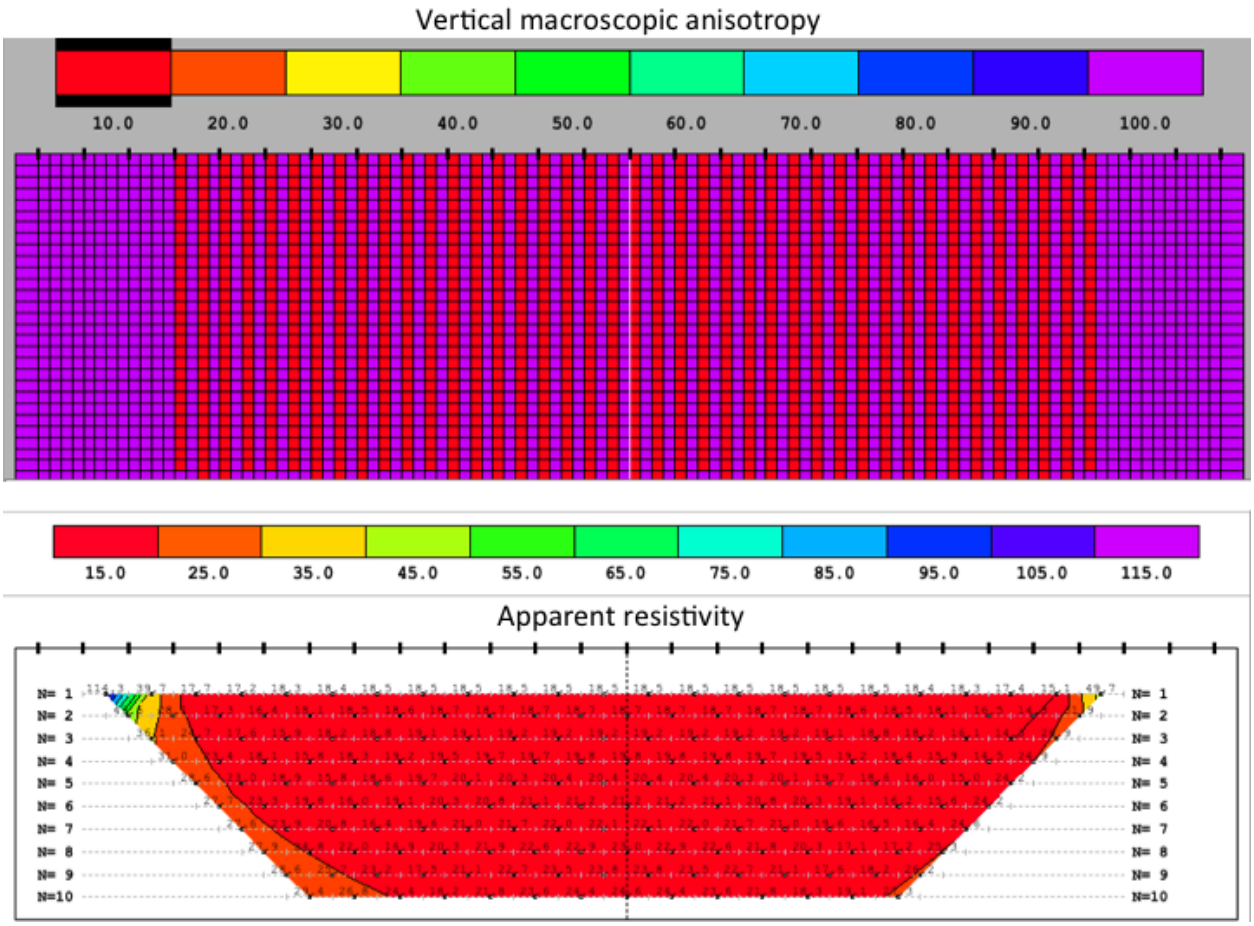

Figure 4.6.12b

Return to top

Solutions for arbitrary resistivity distribution

There are very few simple analytical expressions for the potential for the potential distribution for non-layered models and unfortunately there are very few geological situations for which the layered model is applicable. The solutions for potentials in a general inhomogeneous half-space must be obtained using numerical models based on discrete gridded representations of the subsurface. These are described in the next section.

One useful analytical model is that of a vertical contact between two homogeneous quarter spaces as illustrated in Figure 4.6.13. The solution for a point source near a vertical contact is described in an earlier section. The solution can be invoked two calculate the potentials and hence the apparent resistivity for the dipole-dipole array shown below.

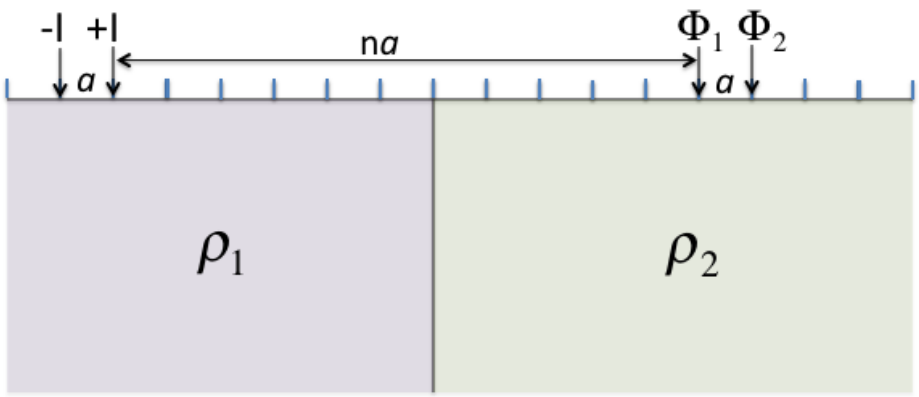

Figure 4.6.13

The equation for the apparent resistivity of the dipole-dipole array is:

$$\rho_a = \frac{V}{I} \pi \ a \ n(n+1)(n+2)$$

so if we calculate the potentials from the vertical contact solution, calculate V from Φ_1-Φ_2 we can then calculate ρ_a.

The solutions for the potentials on the side opposite the vertical contact are given by:

$$\Phi_1 \text{ due to } +\text{I} = \frac{I\rho_2(1-k)}{2\pi na}$$

$$\Phi_1 \text{ due to -I} = \frac{-I\rho_2(1-k)}{2\pi(na+a)}$$

$$\Phi_2 \text{ due to +I} = \frac{I\rho_2(1-k)}{2\pi(na+a)}$$

$$\Phi_2 \text{ due to -I} = \frac{I\rho_2(1-k)}{2\pi(na+2a)}$$

where $k = \dfrac{\rho_2 - \rho_1}{\rho_2 + \rho_1}$.

With this value of k the voltage on the potential electrodes is then:

$$V = \Phi_1 - \Phi_2 = \frac{I\rho_2(1-k)}{2\pi a}\left[\frac{1}{n} - \frac{1}{(n+1)} - \frac{1}{(n+1)} - \frac{1}{(n+1)}\right]$$

$$V = \frac{I\rho_2(1-k)}{\pi a}\frac{1}{n(n+1)(n+2)}$$

Substituting this value for V in the expression for apparent resistivity for the dipole-dipole array yields:

$$\rho_a = (1-k)\rho_2 \quad \text{a constant.}$$

This explains the form of the pseudo-section in Figure 4.6.4b in which the triangular zone in the center is constant. With $\rho_2 = 100$ and $\rho_1 = 100$, k=0.818 and so with this value of k, ρ_a is 18.2 as seen in the pseudo section.

Another useful model, described by Van Nostrand (1953), is for the response of an expanding Wenner array centered above a perfectly conducting sphere as illustrated in Figure 4.6.14.

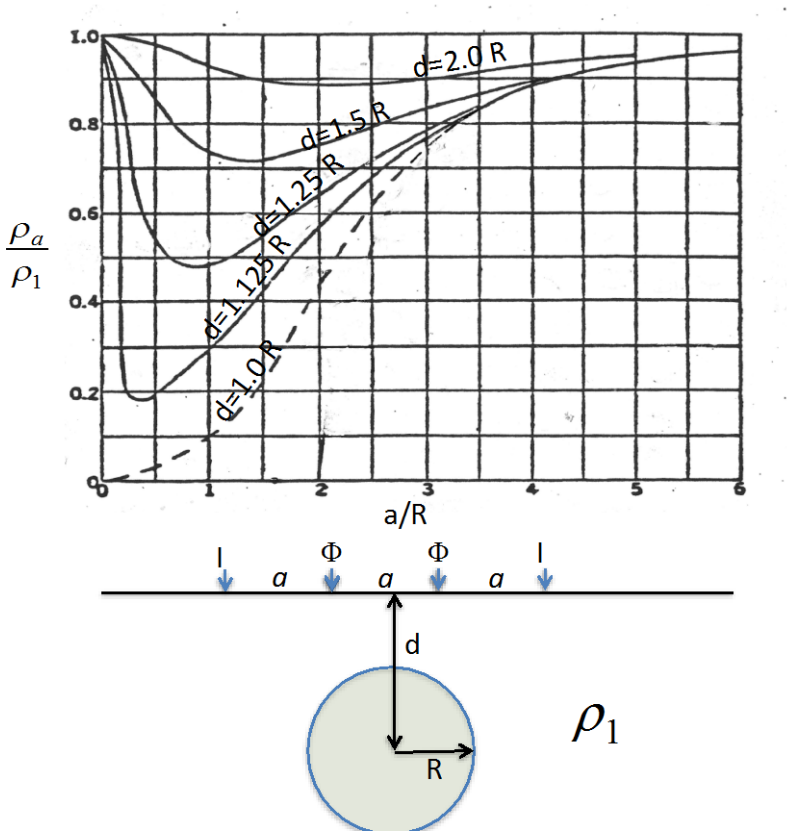

Figure 4.6.14

This model is important because it sets a limit on the depth of detection of a conducting object for a resistivity array. Given the inescapable effects of near surface inhomogeneities discussed above, it is unlikely that relative changes in the apparent resistivity 'anomaly' of less than 10% would be detectable along a profile of soundings, so the maximum depth of detection for such a target for the Wenner array would be a little better than two times the depth of burial.

The sphere is a useful model for quantitatively studying the basic properties of the secondary fields produced on the surface by a finite body at variable depth and in a variety of source fields, and for obtaining estimates of the practical magnitude of

the source currents needed. A schematic of a typical model for a buried sphere is shown in the sketch of Figure 4.6.15.

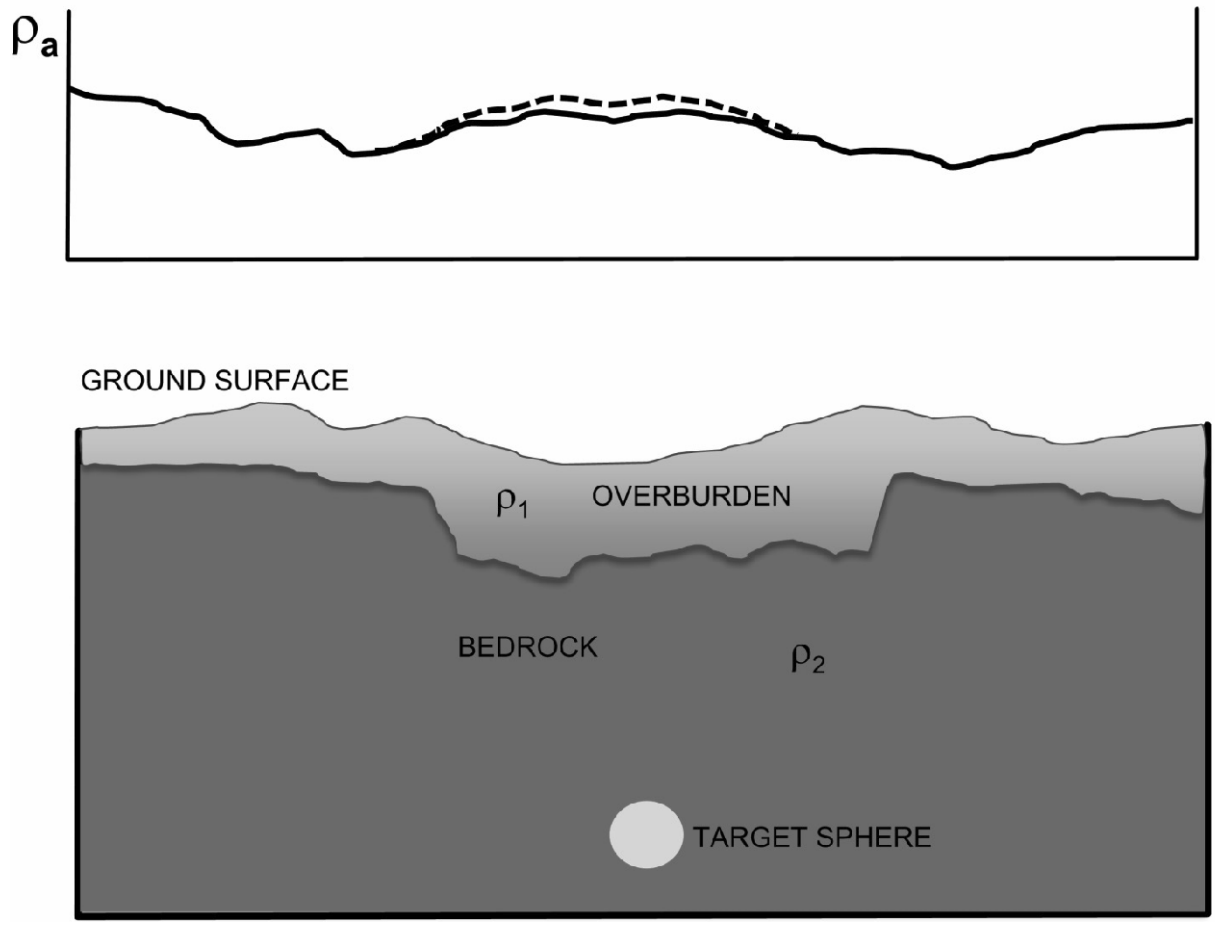

Figure 4.6.15

The solution for the fields of a buried sphere from surface dipole sources on the surface is a challenging numerical problem except using the limiting solution by Van Nostrand given above. An approximate solution is described below that captures the key elements of the response of a sphere Figure 4.6.16.

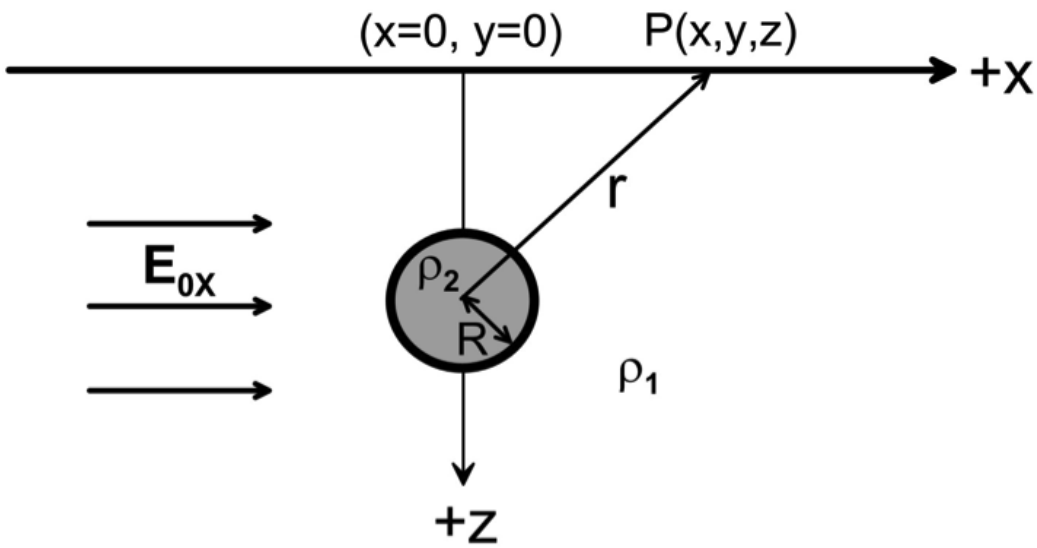

Figure 4.6.16

The expression for the secondary or anomalous potential at an observation point P arising from a spherical body of resistivity ρ_2 and radius R in a whole space of resistivity ρ_1 and in a uniform inducing field E_{0x}, is given by Ward (1967):

$$\phi^a = \frac{\rho_1 - \rho_2}{\rho_1 + 2\rho_2} E_{0X} R^3 \frac{1}{r^2} \cos\theta$$

The potential of a simple current dipole of moment $p = I\,dL$ in a medium of resistivity ρ_1 is $\frac{p\,\rho_1}{4\pi}\frac{\cos\theta}{r^2}$, so the solution for a finite radius sphere is given by an equivalent dipole of moment of

$$p = I\,dL = \frac{\rho_1 - \rho_2}{\rho_1 + 2\rho_2} \frac{E_{0X}\,4\pi R^3}{\rho_1}$$

This is a quantitative statement of the non-uniqueness problem: the external field only depends on the product of the size term and the resistivity contrast term. The

expression also shows the saturation effect; the moment reaches a limit of $\frac{E_{0X}4\pi R^3}{\rho_1}$ when $\rho_2 << \rho_1$, and half that and of the opposite sign, i.e., $-\frac{E_{0X}4\pi R^3}{2\rho_1}$ when $\rho_2 >> \rho_1$. This phenomenon is characteristic of the anomalies of all finite bodies; the anomaly reaches an asymptotic value by the time the contrast exceeds 30 or so. Generally, the horizontal component of the electric field E_X is measured on a line over the sphere, so taking the x component of the negative gradient of the potential yields the following expression for E_X on a profile, a distance z above the sphere:

$$E_X = \frac{\rho_1 - \rho_2}{\rho_1 + 2\rho_2} E_{0X} R^3 \left[\frac{2x^2 - y^2 - z^2}{r^5} \right]$$

The maximum secondary field anomaly occurs directly above the sphere at x=0, y=0, and at –z, so the peak anomaly is:

$$E_X = \frac{\rho_1 - \rho_2}{\rho_1 + 2\rho_2} \frac{E_{0X} R^3}{z^3}$$

The above expressions were derived for a sphere in a conducting whole space. If the sphere was in a half-space whose surface was defined by the solid profile line in Figure 4.6.15, an approximate solution for the horizontal electric fields on the surface can be obtained by superimposing the solution for a second sphere an equal distance above the surface: this approximately doubles the surface fields. If the target sphere is resistive and with the above approximation and assuming a very high contrast the anomaly becomes:

$$E_X = E_{0X} \left(\frac{R}{z} \right)^3 .$$

For a given sphere radius the anomaly falls off as the inverse cube of the depth. The anomaly must be measured in the presence of the primary field, so there will

be some measuring instrument limitation on the smallest ratio of E_X / E_{0X} that can be resolved. More important is the fact that the background half-space is generally not uniform nor is the ground surface a flat plane. The surface electric field will be highly variable due to near surface resistivity inhomogeneities and topography, and this background 'geologic noise' will determine the limit for detecting the sphere.

A typical shallow geologic section has an irregular surface of a variable thickness overburden on an underlying bedrock formation. The surface electric fields, converted to apparent resistivity, ρ_a, are irregular and their perturbation by a target sphere at depth, shown by the dashed line profile in Figure 4.6.15, is very small. From a mapping point of view it is unlikely that changes in ρ_a or E_X / E_{0X} of less than 1.0 % could be identified as a target. This implies that R/z would have to be greater than $\sqrt[3]{10^{-2}}$ or ~0.22 to be detected. For a 50 m sphere the depth of detection would be limited to ~230 m. Somewhat counter intuitively a perfectly conducting sphere of the same radius could be detected to ~290 m. This simple model illustrates the fundamental limitation of any resistivity method for detecting resistivity anomalies at depths much greater than three times their dimension. However, for monitoring changes in the size of such a target over time, the full sensitivity of the measurements can be used, since the background surface electric field can be assumed constant, and so differences highlight the anomaly. The derivation above assumes that the incident electric field is constant with depth and uniform across the sphere. In fact, the field from any finite current source would decrease with depth so that the induced dipole moment in the sphere would also decrease with depth and so the anomaly would fall off faster than $1/r^3$. Further, since the size of the anomaly depends on the amplitude of the inducing field at the sphere, a more complete analysis for a representative source must be made to

determine the currents that would be necessary to probe to a desired depth. To this end the horizontal field at the midpoint of the bipole of Figure 4.5.17, given a length L, versus depth is calculated via Telford et al. [1990]:

$$E_{0X}(z) = \frac{I\rho_1}{2\pi} \frac{L}{\left(z^2 + \frac{L^2}{4}\right)^{3/2}}.$$

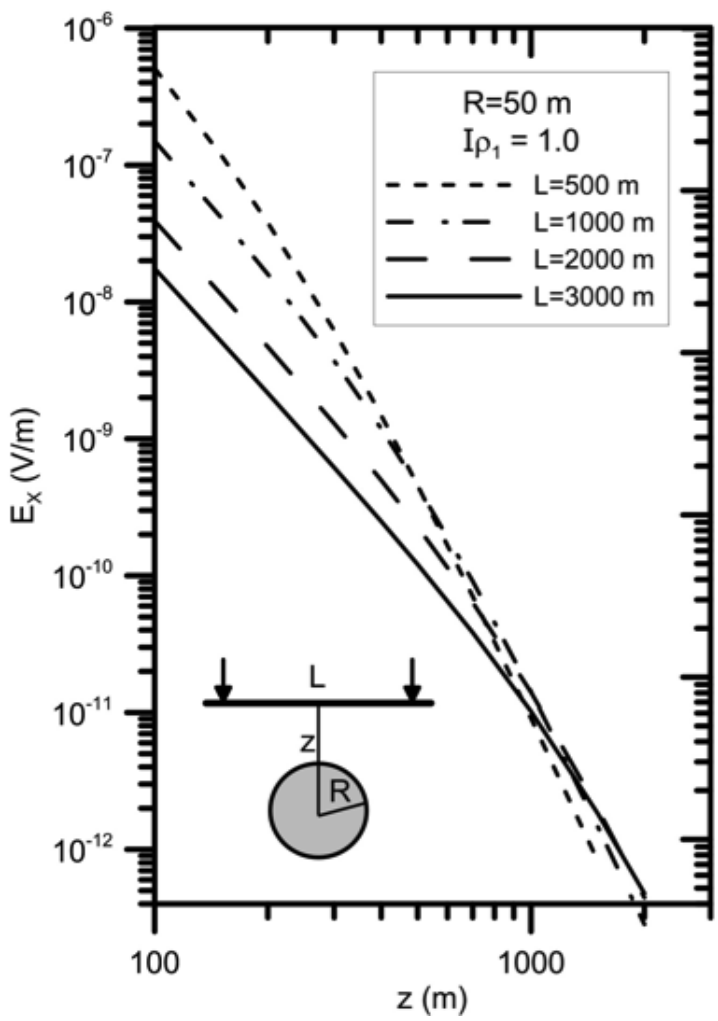

Figure 4.6.17

At depths greater than the diameter of the sphere and for values of L greater than the depth of the sphere it can be assumed that this incident field is uniform across

the sphere and this value of E_{0X} can be substituted in the equation above to find the anomalous E_X back at the surface. It is clear from this equation that for a constant current the field decreases with increasing L and increasing z. Furthermore, when L << z the field falls off as $1/z^3$ and so the anomalous field falls off as $1/z^6$. For L >> z the field falls off as $1/L^2$ and then the anomalous field falls as $1/z^3$ as it would in a uniform field. These effects are most easily seen graphically in Figure 4.6.17, a plot of the anomalous horizontal field at the surface for a resistive sphere of 50 m radius versus depth of burial for a range of bipole lengths L, and $I\rho_1 = 1.0$.

In field surveys, the sensitivity limit is set by the noise level of the voltage measuring electrodes. For carefully installed metal-electrolyte electrodes and for capacitive electrodes this noise level is about $10^{-7} V/\sqrt{Hz}$ at 1.0 Hz. For a 100 m receiving dipole the field noise level would thus be $10^{-10} V/m/\sqrt{Hz}$. To resolve an anomaly, its amplitude should probably be ten-times the noise so a detectable anomaly must have an amplitude of $10^{-9} V/m/\sqrt{Hz}$. Field transmitters can deliver 100 Amps into contacting metal sheet electrodes, and using 10 Ohm-m for a representative half-space gives $I\rho_1 = 1000$. Referring to Figure 15 the detection threshold is at 10^{-12} V/m and the maximum depth of detection is ~1.5 km with a 3 km transmitting bipole. Doubling the radius of the sphere to 100 m increases the maximum depth of detection to 2.5 km.

In practice, the surface anomalous field must be measured in the presence of the primary field – the field on the surface from the current electrodes emplaced on the background half-space $E_X^{Z=0}$. With a 20-bit voltage receiver the minimum resolvable signal would then be ~$10^{-6} \times E_X^{Z=0}$. A useful measurement signal should probably be ten-times this value. A plot of the anomalous signal from the 50 m test

sphere normalized by the primary field is presented in Figure 4.6.18 as a function of the depth of the sphere for a variety of bipole lengths L.

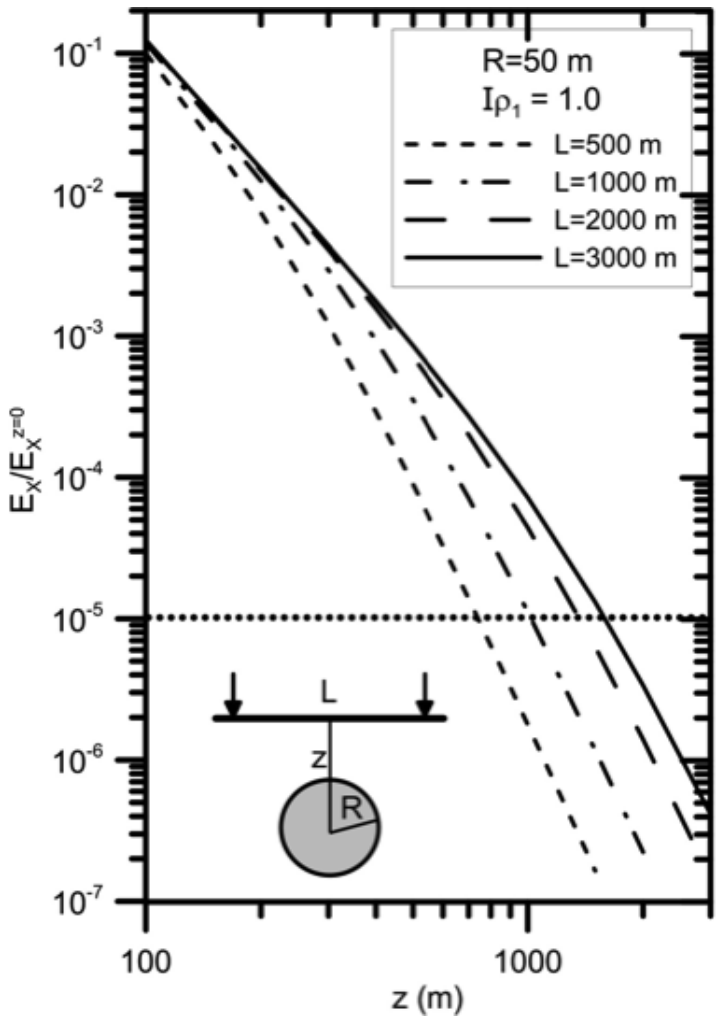

Figure 4.6.18

With this criterion it appears that the 50 m sphere could be well resolved to 1.5 km depth with a 3 km bipole. Note that on the basis of signal strength the maximum depth of detection is almost 1.5 km for all values of L but for short bipoles the dynamic range limit is exceeded at much shallower depths. This is another way of stating that the best detectability is achieved as the bipole length increases and the incident fields become uniform with depth.

Return to top

The general two-dimensional model

The model of a general inhomogeneous distribution of resistivity is solved using a numerical method in which the subsurface is discretized with a two or three dimensional grid and the governing equations for potential are enforced at each point on the grid leading to a very large set of simultaneous equations. A brief description of this process, applied to a two dimensional model, taken from Dey and Morrison (1979) is presented below. A two dimensional model of the earth is one in which the resistivity variations are confined to a vertical plane perpendicular to the geologic strike: resistivities are constant in the strike direction. A program based on this approach is used for the accompanying program Resis2D.

An example of the approach is illustrated by the small grid shown in Figure 4.6.19.

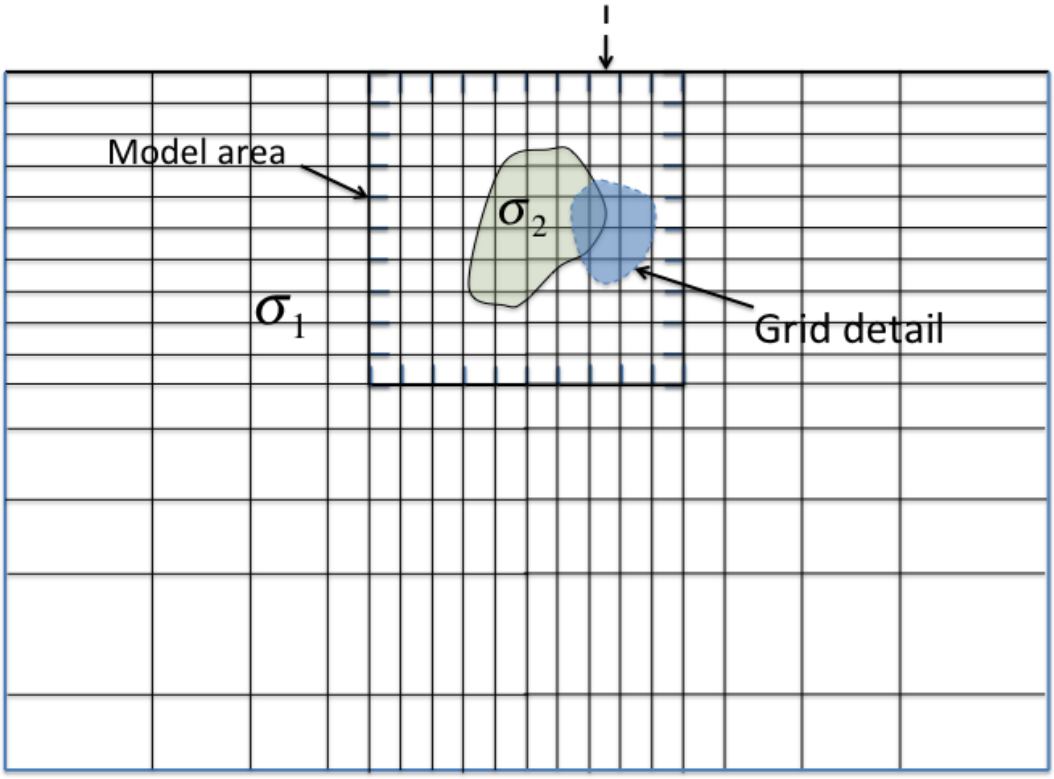

Figure 4.6.19

The intersection points of horizontal and vertical grid lines are the *nodes* of the grid. The nodes are closely spaced in the area of the conductivity anomaly and then spaced increasingly far apart toward the edges of the grid anticipating the fall off of the fields away from the source and the anomalous body.

From the equation of continuity and using Ohm's Law and the fact that $E = -\nabla\Phi$

$$\nabla \cdot J + \frac{\partial \rho}{\partial t} = 0$$

can be written $$\nabla \cdot \left(\sigma \nabla \Phi\right) = \frac{\partial \rho}{\partial t}$$

This can be expanded to:

$$\nabla \sigma \cdot \nabla \Phi + \sigma \nabla^2 \Phi = -\frac{\partial \rho}{\partial t} \delta\left(x_s\right) \delta\left(y_s\right) \delta\left(z_s\right)$$

Using the vector relation

$$\nabla \sigma \cdot \nabla \Phi = \frac{1}{2}\left(-\sigma \nabla^2 \Phi + \nabla^2\left(\sigma \Phi\right) - \Phi \nabla^2 \sigma\right)$$

the equation of continuity finally becomes

$$\begin{aligned} &\nabla^2\left(\sigma\left(x,z\right)\Phi\left(x,y,z\right)\right) + \sigma\left(x,z\right)\nabla^2\Phi\left(x,y,z\right) - \Phi\left(x,y,z\right)\nabla^2\sigma\left(x,z\right) \\ &= -2\frac{\partial \rho}{\partial t}\delta\left(x_s\right)\delta\left(y_s\right)\delta\left(z_s\right) \end{aligned}$$

where $\delta\left(x_s\right)\delta\left(y_s\right)\delta\left(z_s\right)$ are the Dirac delta functions that locate the point creation (injection) of charge at the source coordinates x_s ,y_s, z_s. A source of current, I, coulombs per second, is equivalent to the above $\frac{\partial \rho}{\partial t}$.

The ∇^2 operators now must be approximated by their finite differences between the nodes of the grid. To illustrate how this is done consider the two-dimensional approximation to $\frac{\partial^2\Phi}{\partial x^2}+\frac{\partial^2\Phi}{\partial y^2}=0$ using the node convention for the grid detail of Figure 4.6.20.

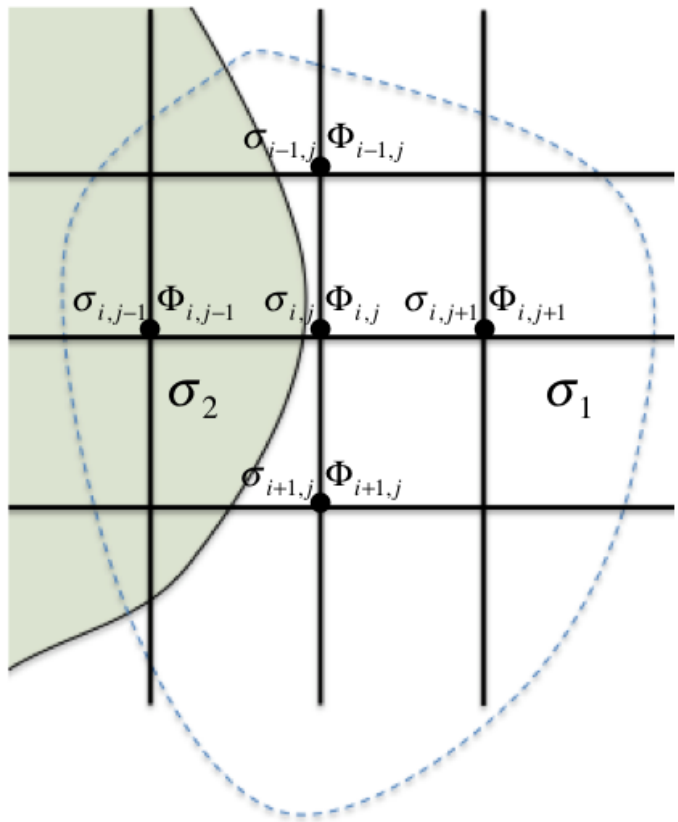

Figure 4.6.20

Assume a grid spacing of r. Then

$$\frac{\partial^2\Phi}{\partial x^2}+\frac{\partial^2\Phi}{\partial x^2}\approx\frac{\left(\frac{\Phi_{i,j+1}-\Phi_{i,j}}{r}\right)-\left(\frac{\Phi_{i,j}-\Phi_{i,j-1}}{r}\right)}{r}+\frac{\left(\frac{\Phi_{i-1,j}-\Phi_{i,j}}{r}\right)-\left(\frac{\Phi_{i,j}-\Phi_{i+1,j}}{r}\right)}{r}$$

so $\nabla^2\Phi=0$ yields an expression for $\Phi_{i,j}$

$$\Phi_{i,j} = \frac{\Phi_{i,j+1} + \Phi_{i,j-1} + \Phi_{i-1,j} + \Phi_{i+1,j}}{4}$$

The potential at the 'central' node is the average of the surrounding nodes. This finite difference operation is then applied to all the ∇^2 terms in the above equation of continuity, noting that the equation is equal to the source term, I, at the node of current injection , and a rather large collection of equations are collected for the potential at node *i,j*. The process is repeated for every node and a large set of equations is assembled for the potentials at every node in terms of the surrounding potentials and conductivities and the source. These equations can be organized as a large matrix equation:

$$\|C\| \cdot \|\Phi\| = \|I\|$$

The desired solution is then obtained by inverting C to yield:

$$\|\Phi\| = \|C\|^{-1} |I|.$$

The inversion of C is non-trivial because for a practical grid there may be thousands of nodes.

<u>Two-dimensional models from Resis2D</u>

Figure 4.6.21 is a model of a simple two-layer geology overlying a vertical conductive dike (upper pseudo-section panel) and overlying the same dike but now resistive (lower panel).

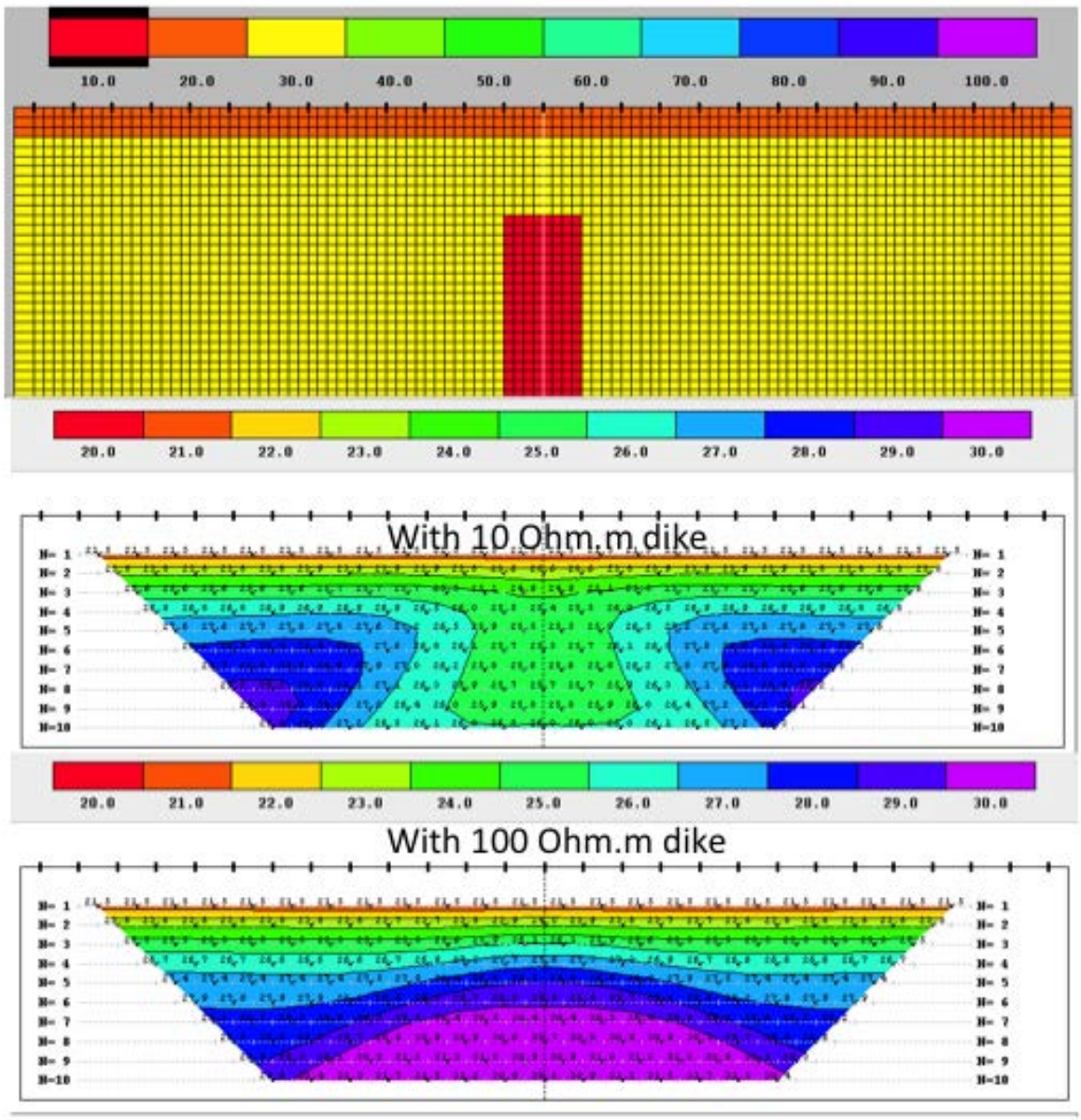

Figure 4.6.21

Figure 4.6.22 shows the pseudo-section for the same conductive dike model but with a thin resistive slab on the surface.

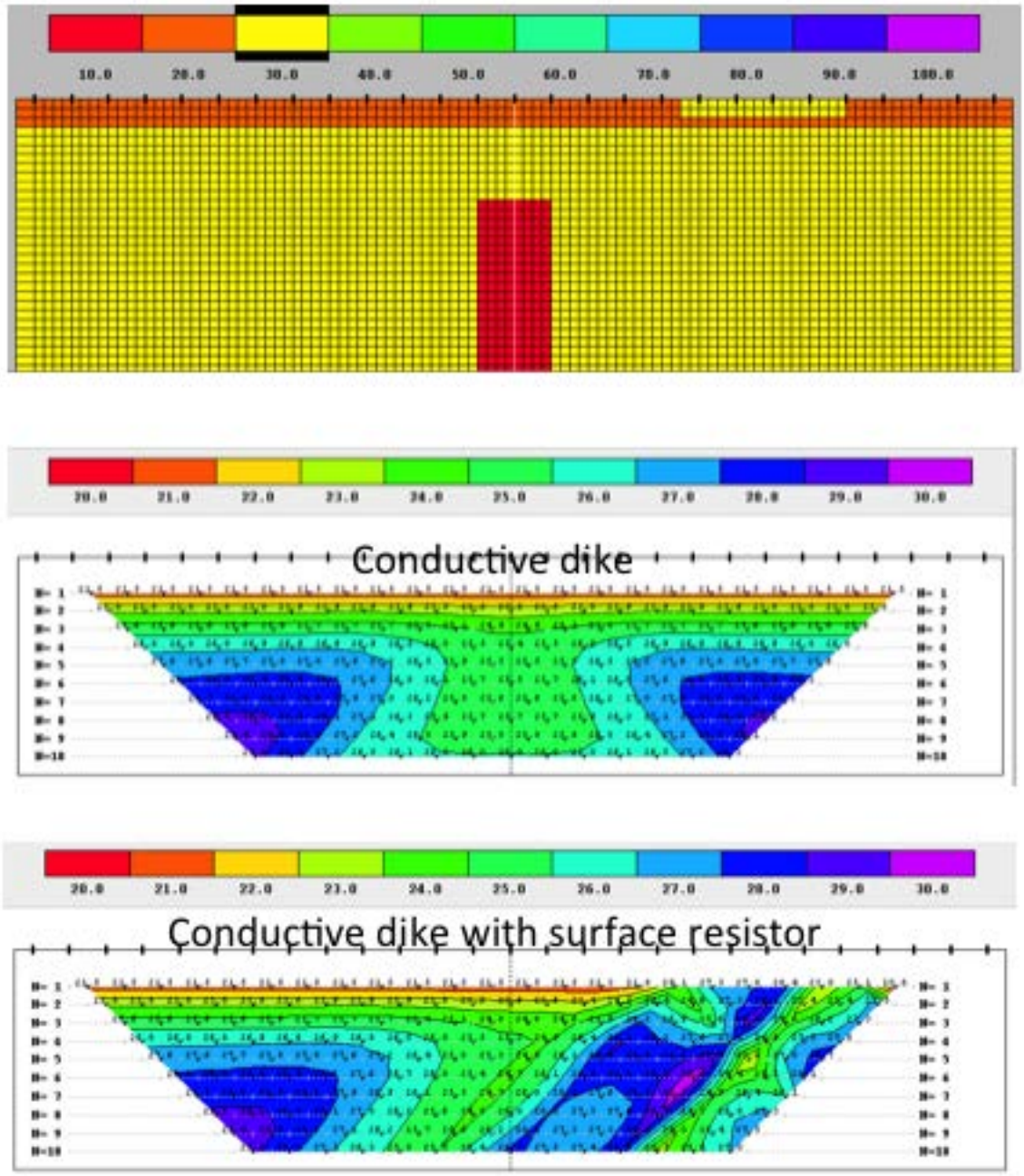

Figure 4.6.22

In a study to determine whether a surface resistivity technique could be used to monitor the injection of a slab like plume of liquid CO_2 the simple model of Figure 4.6.23 was used to simulate the expected plume (Gasperikova and Morrison,

2018). This is a two-dimensional model, infinite in the y-direction. The slab is 50 m thick, 400 m in lateral extent, at a depth of 1.0 km. The body was given the expected high resistivity for CO_2 and for comparison a low resistivity of 1.0 Ohm-m. The response of the thin resistive slab of finite lateral extent is significantly less than that of the conductive slab. The response in Figure 4.6.23 is for a traversing dipole-dipole array. The dipole-dipole array combines sounding and lateral resolution, and has a significant deployment advantage in that cable needs only be laid between relatively closely spaced electrodes – depth of detection is achieved by increasing the dipole separation. Each dipole is 200 m long and the separation is kept at 2 km as the array moves in 200 m increments over the body. The apparent resistivities are plotted at the midpoint of the array for a conductive body and a resistive body. The saturation, a maximum response, occurs for $\rho_2 \geq 10\rho_1$ for the resistive body, but only for $\rho_2 \leq 0.03\rho_1$ for the conductive body. The conductive slab brings the apparent resistivity down by 7%, but the resistive slab increases it only by 1.6%. The resistive finite lens of CO_2 would be very difficult to detect or to monitor.

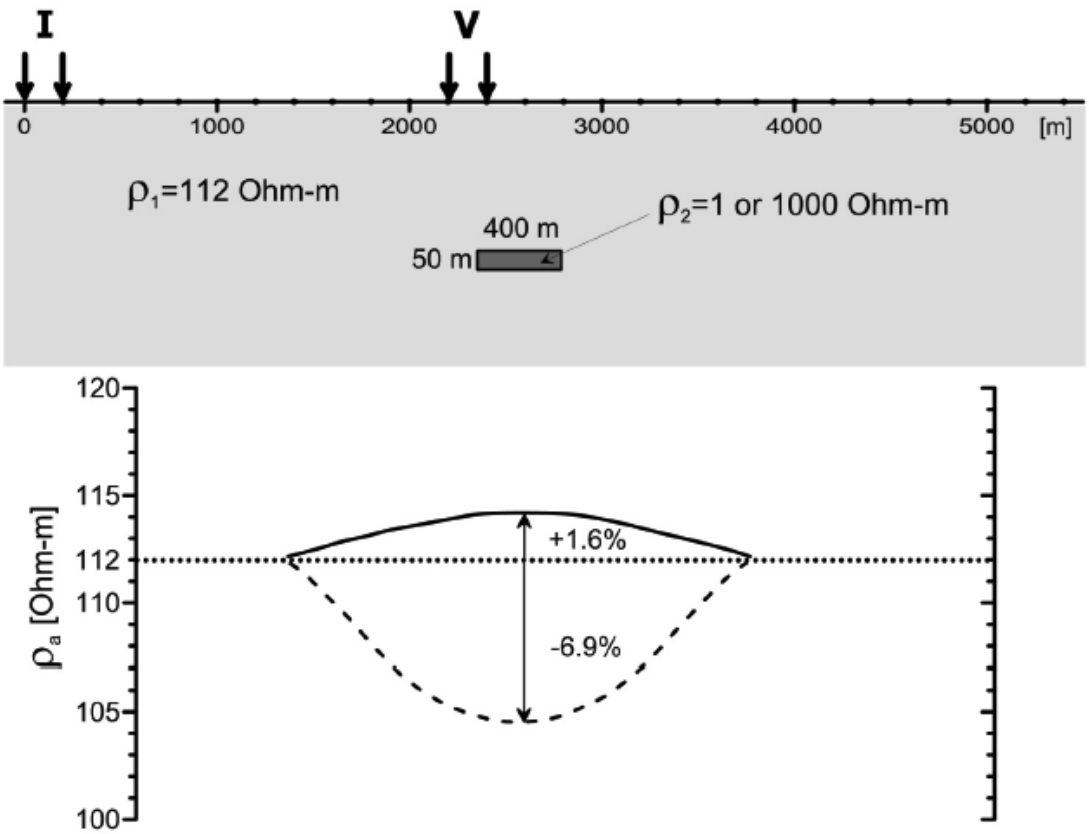
I
V
0
1000
2000
3000
4000
5000
[m]
ρ1=112 Ohm-m
ρ2=1 or 1000 Ohm-m
400 m
50 m
120
115
112
110
105
100
ρa [Ohm-m]
+1.6%
-6.9%

Figure 4.6.23